ÉCOLE DE TECHNOLOGIE SUPÉRIEURE
UNIVERSITÉ DU QUÉBEC

THESIS PRESENTED TO
ÉCOLE DE TECHNOLOGIE SUPÉRIEURE

IN PARTIAL FULFILLMENT OF THE REQUIREMENTS FOR
A MASTER'S DEGREE IN MECHANICAL ENGINEERING
M. A. Sc.

BY
Hong Den NGUYEN

NUMERICAL SIMULATION OF FORMING OF THERMOPLASTIC COMPOSITES PPS / CARBON FIBER

MONTREAL, SEPTEMBER 28, 2015

© Copyright 2015 reserved by Hong Den Nguyen

© Copyright

Reproduction, saving or sharing of the content of this document, in whole or in part, is prohibited. A reader who wishes to print this document or save it on any medium must first obtain the author's permission.

BOARD OF EXAMINERS

THIS THESIS HAS BEEN EVALUATED

BY THE FOLLOWING BOARD OF EXAMINERS:

Professor Zhaoheng Liu, President of the jury
Mechanical Engineering Department, École de technologie supérieure

Professor Ricardo Zednik, Jury member, Examiner
Mechanical Engineering Department, École de technologie supérieure

Professor Tan Pham, Jury member, Thesis supervisor
Mechanical Engineering Department, École de technologie supérieure

THIS THESIS WAS PRENSENTED AND DEFENDED

IN THE PRESENCE OF A BOARD OF EXAMINERS AND THE PUBLIC

ON SEPTEMBER 24 2015

AT ÉCOLE DE TECHNOLOGIE SUPÉRIEURE

ACKNOWLEDGMENTS

I would like to express my deep gratitude to Professor Tan Pham, my research supervisor, for his patient guidance, enthusiastic encouragement and useful critiques of this work. My research project would not have been finished without the precious support that I received from my director.

I would like to thank my thesis committee members: Professor Liu, Professor Zednik, for their evaluation, insightful comments and questions.

I also gratefully acknowledge all the partners who collaborated to this project: Professor Hoa Van Suong and his Ph.D. student, Amir Bahram Kaganj, from Concordia university, Professor Martine Dubé and her Master's student, Thibault Jamin from École de Technologie supérieure, Stéphane Héroux from Delastek company and all partners from Bombardier company and Canada National Research Council.

I would like to thank the technicians of the laboratory of the mechanical department for their help in using technical equipment that supported my research work.

I would also like to extend my thanks to Dr. René Ten Thije and Dr. Sebastiaan Haanappel from University of Twente, for supporting me in my use of Aniform software.

Finally, I must sincerely thank my family and my friends for their encouragement during the tough times when I live very far from them, and from my country.

SIMULATION NUMÉRIQUE DU FORMAGE DES COMPOSITES THERMOPLASTIQUES PPS/FIBRE CARBONE

Hong Den NGUYEN

RÉSUMÉ

Cette recherche a pour but la modélisation du procédé de formage par estampage des composites thermoplastiques pour prédire les distorsions de forme lors du formage tel que les rides, l'orientation des fibres et la distribution des épaisseurs. Le formage de stratifié multicouche de composites de polysulfure de phénylène et fibre de carbone (PPS/CF) a été réalisé avec succès pour plusieurs géométries de simples formes à des complexes. Les mécanismes de déformation primaires du matériau PPS/CF ont été étudiés dans cette recherche. Les modèles numériques qui pourraient prendre en compte ces mécanismes de déformation ont été déterminés. Une bonne combinaison des modèles numériques primaires pour la prédiction de formation a été étudiée dans cette étude. Le cisaillement intra-pli, la flexion et la logique de contact entre les plis individuels et entre outil-pli ont été bien considérés dans ce travail. Les effets de frottement entre outil/plis et entre les plis sur la qualité du formage ont été particulièrement étudiés. Les différences entre les résultats expérimentaux et les résultats numériques en termes d'épaisseur, d'orientation des fibres et de distribution de rides ont été minimisées en utilisant une technique d'optimisation multi-objectif pour identifier les paramètres du modèle de matériau. Un bon accord a été trouvé entre les résultats expérimentaux et la prédiction numérique. Les données obtenues, y compris les paramètres de matériaux optimisés et la bonne combinaison de modèles numériques ont été appliquées pour simuler le formage de plusieurs autres géométries et de différentes séquences d'empilement de stratifiés. Dans cette recherche, les simulations numériques ont été utilisées avec succès comme un outil efficace et à faible coût pour la conception optimisée des moules pour l'estampage des matériaux composites thermoplastiques PPS/CF.

Mots-clés: Composites, modélisation, thermoplastiques, optimisation, simulation, formage-estampage

NUMERICAL SIMULATION OF FORMING OF THERMOPLASTIC COMPOSITES PPS/ CARBON FIBER

Hong Den NGUYEN

ABSTRACT

This research aims to model the stamp-forming process of polyphenylene sulfide/carbon fiber (PPS/CF) thermoplastic composite to predict the shape distortions during the forming process, such as wrinkles, fiber orientations and thickness distribution. Forming simulations and experiments of multi-layer laminates of PPS/CF composites were successfully performed for several geometries from simple to complex shapes. The primary deformation mechanisms of PPS/CF material were examined in this study. Numerical models that could take into account these mechanisms were determined. A good combination of primary numerical models used for stamp-forming prediction was investigated. Intra-ply shear, bending behaviours and the contact logic between the individual plies and between tool-ply were considered in this work. The effects of friction between tool/ply and between ply/ply on the quality of stamp forming were investigated. The differences between experimental and numerical results in terms of thickness, shear-angle and wrinkle distributions were minimized using a multi-objective optimization technique to identify the material parameters used for forming simulations. A good agreement was found between the experimental results and the predicted results. The obtained data including the optimized material parameters and the best numerical model combination were applied for the stamp-forming of several other geometries and different laminate stacking sequences. In this research project, forming simulations were successfully used as an efficient and low cost tool for mold design for the stamp-forming of thermoplastic composite PPS/CF materials.

Keywords: Composites, modelling, thermoplastic, optimization, simulation, stamp-forming

TABLE OF CONTENTS

Page

INTRODUCTION 1

CHAPTER 1 LITERATURE REVIEW 3
1.1 Composite materials...3
1.2 Forming in composite manufacturing..3
  1.2.1 Compression moulding of thermoplastic composites 3
  1.2.2 Stamp forming of thermoplastic composites 4
  1.2.3 Vacuum moulding.. 5
  1.2.4 Hydroforming 6
1.3 Deformation mechanisms 7
  1.3.1 Intra-ply shear 7
  1.3.2 Axial loading.. 7
  1.3.3 Ply-tool and ply-ply shear 8
  1.3.4 Ply bending 8
  1.3.5 Compaction/consolidation 9
1.4 Mathematical modelling of thermoplastic composite forming 10
  1.4.1 Isotropic elastic model 10
  1.4.2 Cross viscosity fluid model... 11
  1.4.3 Elastic fiber model 12
  1.4.4 Mooney-Rivlin model.. 12
  1.4.5 Fabric reinforced viscous fluid (FRVF) model.. 13
  1.4.6 Penalty-polymer model 14
  1.4.7 Adhesion model 17

CHAPTER 2 RESEARCH STRATEGY...19
2.1 Research objective 19
2.2 Research strategy 19

CHAPTER 3 FORMING EXPERIMENT OF THE SINGLE CURVATURE SHAPE - PHASE I..23
3.1 Material properties 23
3.2 Experimental process 23

CHAPTER 4 INVERSE CHARACTERIZATION OF MATERIAL PROPERTIES FOR SIMULATION OF STAMP-FORMING OF MULTI-LAYER THERMOPLASTIC PPS/CF COMPOSITES 27
4.1 Introduction...27
4.2 Forming experiment..29
4.3 Deformation mechanisms 31
4.4 The effects of numerical model combinations on forming predictions 32

4.4.1 Numerical models and material properties ... 32
4.4.2 Simulation setup ... 34
4.4.3 Predicted result and experimental validation ... 35
4.5 Inverse material characterization procedure and the effects of material properties on forming predictions ... 39
4.5.1 Simulation-based inverse characterization procedure ... 39
4.5.2 Inverse characterization result analysis ... 41
4.6 Validation of optimized material properties and numerical models in term of wrinkle distribution ... 46
4.7 Conclusions ... 47

CHAPTER 5 SIMULATION-ASSISTED MOULD DESIGN FOR THE FORMING OF PPS/CF COMPOSITE MATERIALS ... 49
5.1 Mould design for the stamp forming of phase II with a ten-layer laminate ... 49
5.1.1 Virtual mould design with numerical parametric study ... 49
5.1.2 Mould design to avoid friction force ... 51
5.2 Mould design for stamp forming of phase III with an eight-layer laminate ... 56

CONCLUSIONS AND PERSPECTIVES ... 61

LIST OF REFERENCES ... 63

LIST OF TABLES

Page

Table 2.1 Laminate setups for three phases 20

Table 3.1 Experimental processing parameters for forming of phase I 25

Table 4.1 Numerical models 33

Table 4.2 Material properties 34

Table 4.3 Material parameters for optimization....41

Table 4.4 Optimization results 45

Table 4.5 Coefficient of determination for evaluating the thickness distribution 46

Table 4.6 Coefficient of determination for evaluating the shear angle distribution ..46

Table 5.1 Virtual mould dimensions....49

Table 5.2 Simulation results....50

LIST OF FIGURES

Page

Figure 1.1 Compression press 4

Figure 1.2 The stamp forming method: (a) heating, (b) the blank in the press, (c) moulding 5

Figure 1.3 Vacuum forming method 5

Figure 1.4 Hydroforming 6

Figure 1.5 Intra-ply shear 7

Figure 1.6 Axial loading 8

Figure 1.7 Tool-ply and ply-ply shear 8

Figure 1.8 Ply bending 9

Figure 1.9 Compaction/consolidation 9

Figure 1.10 A body in initial state and in the deformed state. 12

Figure 1.11 Constant tangential contribution 16

Figure 2.1 Three phases of the project 20

Figure 2.2 Research strategy 21

Figure 3.1 The blank was placed onto the Kapton film. 24

Figure 3.2 The mould was fully closed 24

Figure 3.3 The formed part 25

Figure 4.1 Stamp forming system 30

Figure 4.2 Blank is in the oven 30

Figure 4.3 The formed part 31

Figure 4.4 Deformation mechanisms 32

Figure 4.5 Simulation setup 35

Figure 4.6 General deformation 36

Figure 4.7 Measurement positions 37

Figure 4.8 Draw lines on the blank 37

Figure 4.9 Thickness distribution..38

Figure 4.10 Shear-angle distribution 38

Figure 4.11 Simulation-based inverse characterization procedure 40

Figure 4.12 Optimization iteration history plot for $F(x, y)$ 42

Figure 4.13 Thickness comparison between iterations 43

Figure 4.14 Thickness difference between the predicted results and the experimental results 43

Figure 4.15 Shear angle comparison between iterations..44

Figure 4.16 Shear angle difference between the predicted results and the experimental results 44

Figure 4.17 Wrinkle comparison between the experimental and predicted results of the ten-layer part...47

Figure 4.18 Wrinkle comparison between the experimental and predicted results of the four-layer part 47

Figure 5.1 Mould geometry...50

Figure 5.2 Simulation setup of mould C 51

Figure 5.3 Forming predicted results of the mould C: (a) Shear angle; (b) Thickness51

Figure 5.4 Mould C2 52

Figure 5.5 Simulation setup for mould C2 52

Figure 5.6 Forming prediction of the mould C2: (a) Shear angle; (b) Thickness 53

Figure 5.7 Real mould design (a) Two half- moulds; (b) The mould installed in the press 53

Figure 5.8 Pin locations...54

Figure 5.9 Simulation setup: (a) Simulation setup; (b) The effect of gravity 54

Figure 5.10 Result comparison: (a) Experiment; (b) Simulation 55
Figure 5.11 Predicted result: (a) Thickness; (b) Shear angle 55
Figure 5.12 Contact between the blank and the mould 56
Figure 5.13 Phase III mould design: (a) Mould design; (b) Virtual formed part 57
Figure 5.14 Forming simulation: (a) Simulation setup; (b) General deformation 57
Figure 5.15 Simulation results: (a) Closed mould; (b) Shear angle values 58
Figure 5.16 Experiment: (a) Forming process, (b) Final shape 59
Figure 5.17 Measurement: (a) Measurement positions; (b) Sample cutting lines 59
Figure 5.18 Thickness comparison 60
Figure 5.19 Shear angle comparison 60

LIST OF ABREVIATIONS

CFRP	Continuous Fiber Reinforced Polymer
CFRTP	Continuous Fiber Reinforced ThermoPlastics
CF	Carbon Fiber
FRVF	Fabric Reinforced Viscous Fluid
CP	Cross-Ply
FE(M)	Finite Element (Method)
FLD	Forming Limit Diagram
LTR	Linear/simplex TRiangular element
PPS	PolyPhenylene Sulfide
QI	Quasi-Isotropic

LIST OF SYMBOLS AND UNITS OF MEASUREMENTS

Scalars

C	Mooney-Rivlin material parameters
E	Young’s modulus, MPa
h	film thickness, mm
I	invariants of the left Cauchy strain tensor
J	Jacobian, volume ratio
ℓ, L	length, mm
p	hydrostatic pressure, MPa
q	scalar weight function
R	radius, mm
R	constraint ratio
T	time, s
u, v, w	displacement in x, y, z directions, mm
V	volume
γ	shear deformation
δ	increment
ε	strain
η	viscosity, MPa·s
ν	volume fraction
ρ	density, 10^3 kg/mm^3
σ	stress, MPa

Vectors

a	fiber direction
n	normal vector
u	displacement, mm
v	velocity, mm/s
X	Lagrangian vector
x	Eulerian vector
τ	interface traction

Tensors

B	left Cauchy-Green strain
C	right Cauchy-Green strain
D	rate of deformation
d	invariant rate of deformation
F	deformation gradient
G	stretch tensor
I	second order unit tensor
σ	Cauchy stress
S	second Piola-Kirchhoff stress

INTRODUCTION

Thermoplastic PPS/Carbon Fiber composite (PPS/CF) is one of the most frequently used thermoplastic composite materials for aircraft structures. It has excellent mechanical properties, high temperature resistance and good chemical resistance. Many advantages of thermoplastic composites are not present in thermoset composites. For example: thermoplastic composites are highly recyclable and can be used for remoulding and reshaping. Thermoplastic composites are also lighter and easier to colour than thermoset materials. Thanks to their advantageous properties, thermoplastic composites are gradually replacing thermoset composites for laminate fabrication, particularly for high volume applications. However, there are a lot of difficulties in stamp-forming thermoplastic composite materials. The process must be performed at an elevated temperature and high pressure. Thermoplastic forming may produce wrinkles and thickness variation in formed parts. High slippages between layers may appear due to the change of friction between tool-ply and between ply-ply. The process becomes much more challenging when dealing with multi-layer laminates and complex mould geometries.

The CRIAQ-COMP512 project was created to study the formability of PPS/CF composite material by stamp-forming. The main objective of this project is to determine the process window for stamp-forming multi-layer PPS/CF material with complex geometries and the limits of the process. The work presented in this master thesis is a part of this project.

This work mainly focussed on the numerical simulation of the stamp-forming process which is necessary to predict shape distortions during the forming process, such as fiber orientations, thickness distribution and wrinkle apparition. Numerical simulations of stamping process were performed using the software Aniform. The work involved four steps: the first step is to determine primary deformation mechanisms during the forming process; the second step is to identify the numerical models that could take into account these deformation mechanisms; the third step is to determine the material parameters for these numerical models; and the final step is to run a new series of numerical simulations using data obtained from the previous steps for new mould design. The content of this Master's thesis is presented in fives chapters and the conclusion as follows:

- Chapter 1: Literature review on composite materials forming;
- Chapter 2: Research strategy;
- Chapter 3: Forming experiment of the single curvature shape;
- Chapter 4: Inverse characterization of material properties for simulation of stamp-forming of multi-layer thermoplastic PPS/CF composites;
- Chapter 5: Simulation-assisted mould design for the forming of PPS/CF composite materials;
- Conclusions and perspectives.

Chapter 1 presented the literature review on composite materials forming, including the modelling works. In Chapter 2, the research strategy was analysed. There were three phases in this research. It started from the forming of a very simple geometry mentioned in Chapter 3 to determine the parameters of the forming process. The second phase was for forming more complex shapes and material stacking sequences. This work was also employed to perform inverse characterization of material parameters using simulation-based multi-objective optimization technique. The study of the second phase was written as a journal article and reproduced as Chapter 4 in this thesis. Chapter 5 presented the mould design assisted by numerical simulations for forming of PPS/CF composites. This part of work was published as a conference paper from which this chapter was reproduced. Finally, the conclusions and perspectives were presented.

CHAPTER 1

LITERATURE REVIEW

1.1 Composite materials

Composite materials are made from two or more constituent materials with significantly different physical or chemical properties that, when combined, produce a material with characteristics different from the individual components. The individual components remain separate and distinct within the final structure. The new material may be preferred for many reasons: stronger, lighter, or less expensive than traditional materials. There are two main categories of constituent materials: matrix and reinforcement. The matrix material surrounds and supports the reinforcement materials by maintaining their relative positions. The reinforcements impart their special mechanical and physical properties to enhance the matrix properties. A synergism produces material properties absent in the individual constituent materials, while the wide variety of matrix and strengthening materials allows the designer of the product or structure to choose an optimum combination (Gibson, 1994).

1.2 Forming in composite manufacturing

1.2.1 Compression moulding of thermoplastic composites

Compression moulding is a forming process whereby a composite material is placed directly into a heated metal mould, softened by the heat, and forced to conform to the shape of the mould as the mould closes. The presses used for compression moulding are manufactured in a wide variety of sizes. Most presses utilize a hydraulic ram in order to produce sufficient force during the moulding operation. The tools consist of a male mould plunger and a female mould. The amount of heat required and instruments necessary to produce the desired product vary. Some plastics require temperature in excess of 700^{o}F (371^{o}C), while others are in the low 200°F (93°C) range. Time is also a factor. Material type, pressure, and part thickness are all factors that will determine how much time the part will need to be in the mould. For thermoplastics, the part and the mould will need to be cooled to an extent, so that the formed part becomes rigid. The force with which the object is compressed will depend on what the object can withstand, particularly in its heated state. For fiber reinforced composite parts being compression moulded, the higher the pressure, the better the consolidation of the laminate, and ultimately the stronger the part. Figure 1.1 shows a compression mould press (Robert *et al.*, 1994).

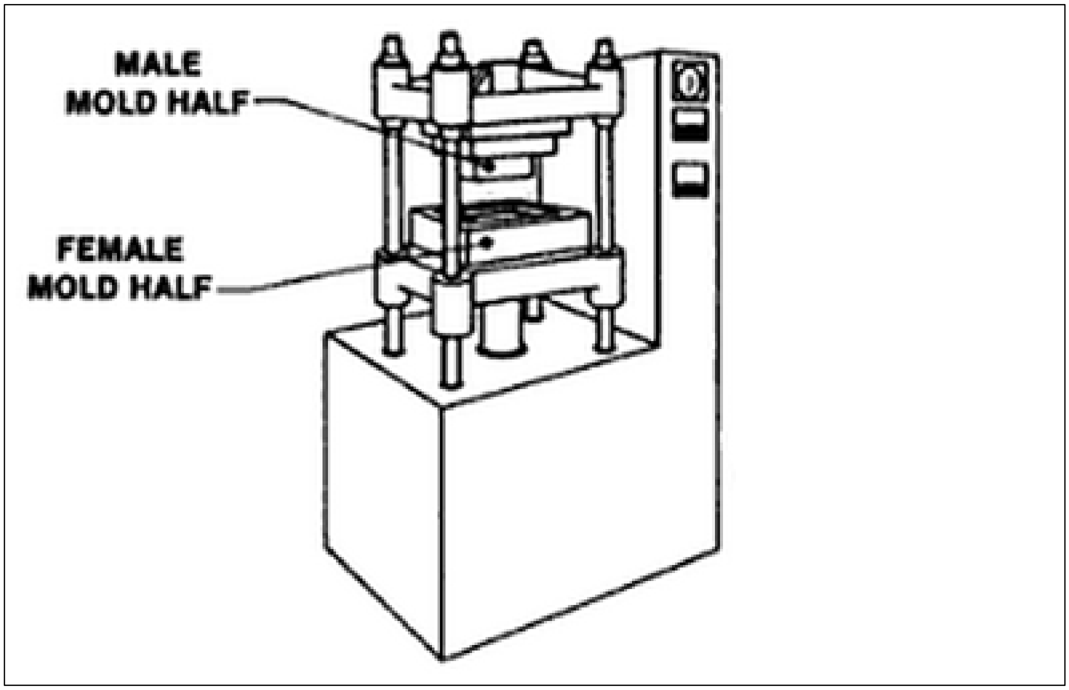

Figure 1.1 Compression press

1.2.2 Stamp forming of thermoplastic composites

In stamp forming, a stack of thermoplastic composites is heated to the softening or melting temperature. The heated stack is then transferred to a moulding press where the laminate is forced into its final shape by a two-part moulding tool. The mould temperatures are maintained constant, below the solidification temperature of the thermoplastic. Figure 1.2 illustrates the stamp forming method (Trudel-Boucher, 2005).

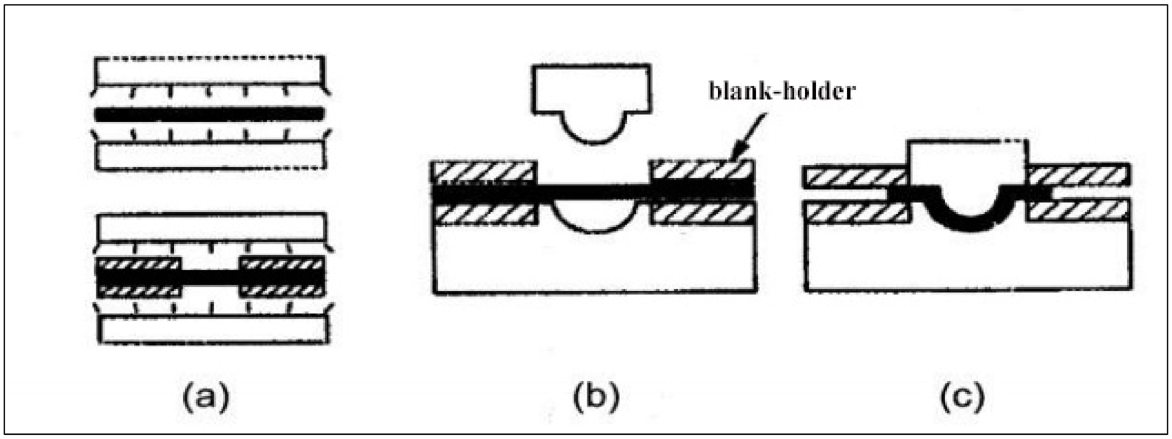

Figure 1.2 The stamp forming method: (a) heating, (b) the blank in the press, (c) moulding

1.2.3 Vacuum moulding

Vacuum moulding is used to make single and/or large composite parts with a one-sided tool and a vacuum bag to form the component. Vacuum forming of thermoplastic composites is a process whereby the laminate is heated to the point that it becomes pliable, allowing it to be formed around a plug or male mould. Vacuum forming of thermoplastic composites has some additional advantages over the traditional forming methods of composite materials: short cycle times, low mould and tooling costs, low machine costs and environmentally friendly production methods (compared to thermoset composites). Figure 1.3 shows the vacuum forming method (Trudel-Boucher, 2005).

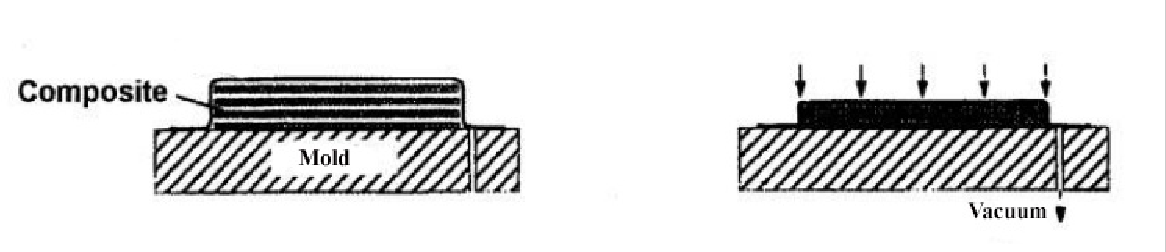

Figure 1.3 Vacuum forming method

1.2.4 Hydroforming

To produce a hydroformed composite part, a diaphragm is lowered onto the blank and an initial fluid pressure is applied that deforms it onto the retracted punch piece. The punch is then extended, forcing the blank material between the punch piece and the pressurized "forming chamber" created as the diaphragm deforms. The punch continues to extend and draws the part until the desired depth and other dimensions are attained. Next, the diaphragm pressure is relieved, and the diaphragm and punch piece are retracted, leaving the formed part to cool and to be processed further. The even hydrostatic pressure applied by the diaphragm helps to prevent fiber wrinkling and other defects. In addition, the diaphragm support also provides for more uniform part thickness and reduces the propensity for part thinning or "necking" as is common in other material drawing processes. The hydroforming schematic is presented in Figure 1.4 (Trudel-Boucher, 2005).

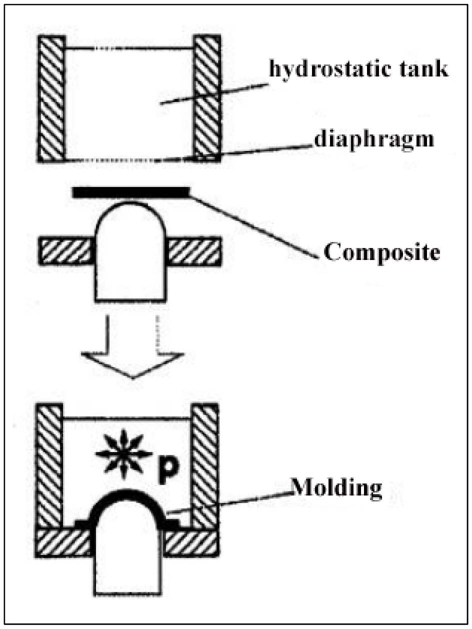

Figure 1.4 Hydroforming

1.3 Deformation mechanisms

This paragraph presents the deformation mechanisms that occur during the forming process of continuous, aligned fiber materials. These have been categorised by several authors (Haanappel, 2013; Long, 2007; Ten Thije, 2007)

1.3.1 Intra-ply shear

Intra-ply shear is usually considered to be the primary deformation mechanism for aligned fiber-based materials. It includes the sliding of parallel tows within a fabric layer or composite ply (longitudinal intra-ply shearing), and rotation of tows at their crossovers (transverse intra-ply shearing) as shown in Figure 1.5 (Haanappel, 2013).

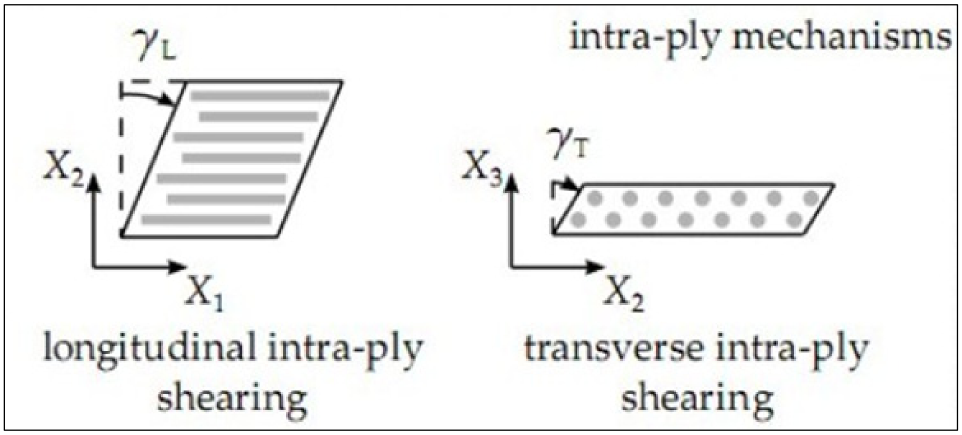
intra-ply mechanisms
γ_L
X_2
X_1
longitudinal intra-ply shearing
γ_T
X_3
X_2
transverse intra-ply shearing

Figure 1.5 Intra-ply shear

1.3.2 Axial loading

The deformation under axial loading is of secondary importance. Loading of aligned fiber based materials along the fiber axis or axes typically results in very large forces and very low maximum strains in comparison to intra-ply shear. The axial loading is illustrated in Figure 1.6 (Haanappel, 2013)

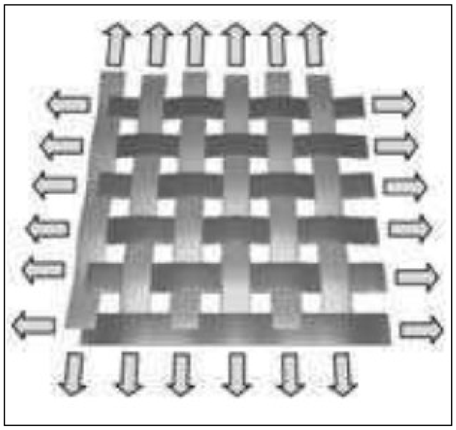

Figure 1.6 Axial loading

1.3.3 Ply-tool and ply-ply shear

During the forming process, friction between the material and forming tools governs the transfer of loads to the material. In multi-layer forming processes, friction between individual layers of material is also of importance. To model forming processes accurately, measurement of friction at ply/tool and ply/ply interfaces is important (Long, 2007). The tool-ply and ply-ply shear is illustrated in Figure 1.7 (Ten Thije, 2007).

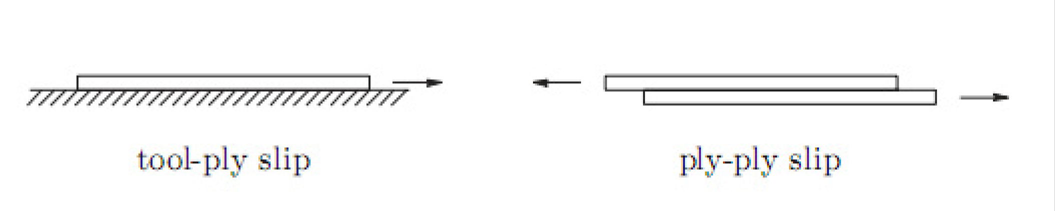

Figure 1.7 Tool-ply and ply-ply shear

1.3.4 Ply bending

The ability of fabric or prepregs to bend out of plane is of course critical for forming of curved components. The bending resistance is usually orders of magnitude lower than intra-ply shear resistance, which in turn is significantly lower than tensile stiffness in the fiber direction (Long, 2007). Figure 4 shows the ply bending behaviours.

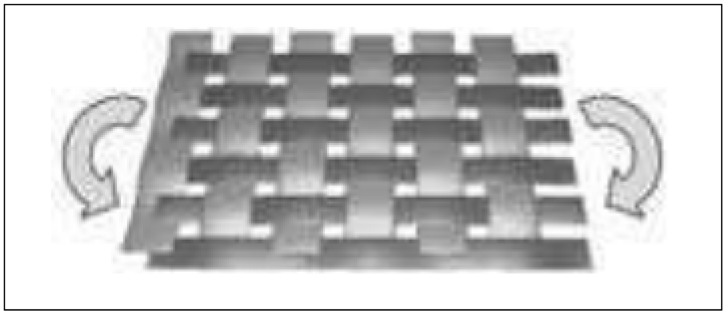

Figure 1.8 Ply bending

1.3.5 Compaction/consolidation

At the end of a forming process, the material must be compacted or consolidated to increase the fiber volume fraction and eliminate voids. For multi-layer, multi-material reinforcement preforms, the compressibility of each material type is likely to be different, so that each layer attains a different fiber volume fraction under the imposed compaction pressure (Long, 2007). Figure 1.9 shows the compaction behaviours.

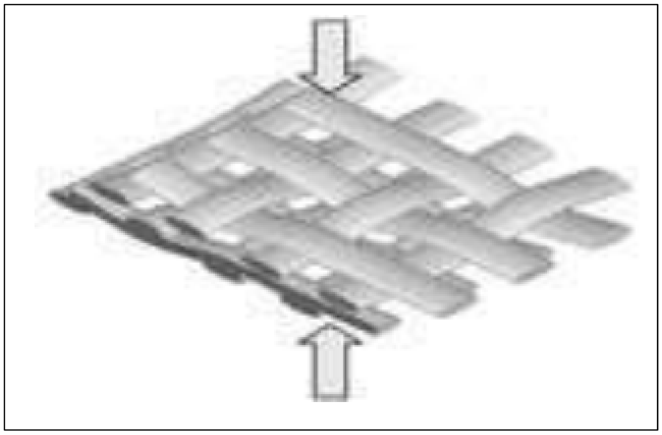

Figure 1.9 Compaction/consolidation

1.4 Mathematical modelling of thermoplastic composite forming

There are many material models which were developed and published recently. This paragraph presents several important models and the parameters used for composite forming simulations.

1.4.1 Isotropic elastic model

Following Hook's law, the second Piola-Kirchhoff stress tensor **S** is calculated as follows (Jones, 1999):

$$\begin{Bmatrix} S_{xx} \\ S_{yy} \\ S_{zz} \\ S_{xy} \\ S_{yz} \\ S_{xz} \end{Bmatrix} = \frac{E}{(1+\nu)(1-2\nu)}[\mathbf{D}]\begin{Bmatrix} \varepsilon_{xx} \\ \varepsilon_{yy} \\ \varepsilon_{zz} \\ \varepsilon_{xy} \\ \varepsilon_{yz} \\ \varepsilon_{xz} \end{Bmatrix} \tag{1.1}$$

with

$$[\mathbf{D}] = \begin{bmatrix} 1-\nu & \nu & \nu & 0 & 0 & 0 \\ \nu & 1-\nu & \nu & 0 & 0 & 0 \\ \nu & \nu & 1-\nu & 0 & 0 & 0 \\ 0 & 0 & 0 & 1-2\nu & 0 & 0 \\ 0 & 0 & 0 & 0 & 1-2\nu & 0 \\ 0 & 0 & 0 & 0 & 0 & 1-2\nu \end{bmatrix} \tag{1.2}$$

and $\{\boldsymbol{\varepsilon}\}$ denotes the Green-Lagrange strain tensor. The relation between the Cauchy stress and the second Piola-Kirchhoff stress is given by:

$$\boldsymbol{\sigma} = \frac{1}{J}.\mathbf{F}.\mathbf{S}.\mathbf{F}^T \tag{1.3}$$

where $\mathbf{F}$ is the deformation gradient tensor and J the Jacobian.

1.4.2 Cross viscosity fluid model

The cross model is a shear rate dependent viscosity model. It is used to model power law type fluids and has a viscosity plateau region at low and high shear rates, respectively. This model was originally developed by Malcom M. Cross in 1965. The Cauchy stress is given by:

$$\boldsymbol{\sigma} = \frac{2\eta(\dot{\gamma})}{J}\mathbf{D} \tag{1.4}$$

where $\mathbf{D}$ is the rate of deformation tensor, J is the Jacobian. The viscosity η depends on the equivalent shear rate $\dot{\gamma}$ and is given by (Cross, 1965):

$$\eta_{(\gamma)} = \frac{\eta_0 - \eta_\infty}{1 + m\dot{\gamma}^{(1-n)}} + \eta_\infty \tag{1.5}$$

where η_0 is the limiting viscosity at zero rate of shear, η_∞ is the limiting viscosity at an infinite rate of shear, m and n are two independent constants and $\dot{\gamma}$ is the rate of shear which is defined as:

$$\dot{\gamma} = \sqrt{(2\mathbf{D} : \mathbf{D})} \tag{1.6}$$

1.4.3 Elastic fiber model

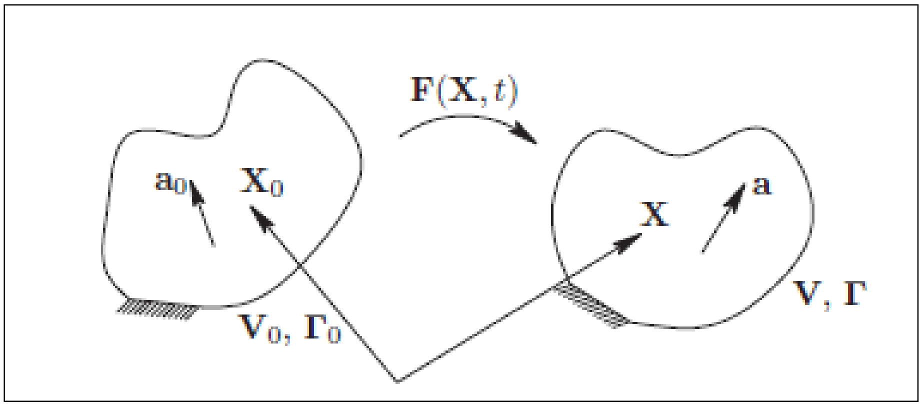

Figure 1.10 A body in initial state and in the deformed state.

Figure 1.10 shows a body in the initial state and in the final deformed state (Ten Thije, 2007). The fiber strain is determined by (Ten Thije, 2014):

$$\boldsymbol{\varepsilon} = \frac{1}{2}\mathbf{a_0 a_0} : (\mathbf{C} - \mathbf{I}) / l_0^2 \tag{1.7}$$

where $\mathbf{a_0}$ is the initial direction vector of the fiber, and l_0 are the initial length of the fiber. Finally, the Cauchy stress tensor is calculated by the following (Ten Thije, 2014):

$$\boldsymbol{\sigma} = \frac{\rho . E_f}{2\rho_0 l_0^4}\mathbf{a a a_0 a_0} : (\mathbf{C} - \mathbf{I}) \tag{1.8}$$

where E_f is the Young's module of fiber and **a** denotes the final direction vector of the fiber.

1.4.4 Mooney-Rivlin model

The Mooney–Rivlin model for hyper-elastic materials is commonly used in connection with simulations of rubber-like or other polymeric structures in, e.g., analytical or finite element contexts. It is based on the work by Mooney (Mooney, 1940), and Rivlin (Rivlin, 1940). The corresponding stress can be expressed as:

$$\mathbf{S}_{ij} = \frac{\partial \mathbf{W}}{\partial \mathbf{E}_{ij}} = 2\frac{\partial \mathbf{W}}{\partial \mathbf{C}_{ij}} \tag{1.9}$$

where $\mathbf{W}$ is the strain energy, $\mathbf{E}$ is the Green strain tensor and $\mathbf{C}$ is the right Cauchy Green deformation tensor. We have the following relationship between $\mathbf{E}$ and $\mathbf{C}$:

$$\mathbf{E} = \frac{1}{2}(\mathbf{C} - \mathbf{I}) \tag{1.10}$$

where $\mathbf{I}$ is the second-order unit tensor. For an isotropic material, $\mathbf{W}$ is given by:

$$\mathbf{W} = \mathbf{W}(\mathbf{I_1}, \mathbf{I_2}, \mathbf{I_3}) \tag{1.11}$$

For an incompressible material, the condition $\mathbf{I_3}=1$ must be fulfilled and then we have the general form as follows:

$$\mathbf{W} = \sum_{i=0}^{\infty}\sum_{i=0}^{n}\mathbf{C}_{ij}(\mathbf{I}_1 - 3)^i(\mathbf{I}_2 - 3)^j \tag{1.12}$$

For the Money-Rivlin model with only two parameters, the Cauchy stress tensor $\boldsymbol{\sigma}$ is given by:

$$\boldsymbol{\sigma} = \frac{1}{\mathbf{J}}.\left(2C_{10}\mathbf{B} - 2C_{01}\mathbf{B}^{-1}\right) \tag{1.13}$$

where C_{10} and C_{01} are two parameters and $\mathbf{B}$ the left Cauchy-Green deformation tensor.

1.4.5 Fabric reinforced viscous fluid (FRVF) model

The fabric reinforced viscous fluid (FRVF) model is a general form for a viscous material with two fiber directions of reinforcement. The Cauchy stress tensor of a FRVF with two fiber directions is determined by (Spencer, 2000):

$$\begin{aligned}\boldsymbol{\sigma} &= -p\mathbf{I} + T_a\mathbf{A} + T_b\mathbf{B} + 2\eta\mathbf{D} + 2\eta_1(\mathbf{A.D} + \mathbf{D.A}) \\ &+2\eta_2(\mathbf{B.D} + \mathbf{D.B}) + 2\eta_3(\mathbf{C.D} + \mathbf{D.C}) + 2\eta_4(\mathbf{C}^{\mathrm{T}}.\mathbf{D} + \mathbf{D.C})\end{aligned} \tag{1.14}$$

where η, η_1, η_2, η_3, η_4 are the viscosities, p the pressure, $\mathbf{D}$ the rate of deformation tensor, T_a and T_b the tensions of fiber respectively in fiber directions $\mathbf{a}$ and $\mathbf{b}$. The viscosities are in general functions of $\mathbf{a}$ and $\mathbf{b}$ which are related to the angle 2Φ between the two fiber directions by:

$$\mathbf{a}.\mathbf{b} = \cos 2\Phi \tag{1.15}$$

The tensors $\mathbf{A}$, $\mathbf{B}$ and $\mathbf{C}$ are given by:

$$\mathbf{A} = \mathbf{a} \otimes \mathbf{a};\ \mathbf{B} = \mathbf{b} \otimes \mathbf{b}\ ;\ \mathbf{C} = \mathbf{a} \otimes \mathbf{b};\ \mathbf{C}^{\mathrm{T}} = \mathbf{a} \otimes \mathbf{b} \tag{1.16}$$

where the symbol $\otimes$ stands for the tensor product, the superscript T denotes the transpose and $\mathbf{a}$, $\mathbf{b}$ denote the actual fiber directions related to the initial directions a_0 and b_0 by:

$$\mathbf{a} = \mathbf{F}.\mathbf{a}_0 \text{ and } \mathbf{b} = \mathbf{F}.\mathbf{b}_0 \tag{1.17}$$

1.4.6 **Penalty-polymer model** (Ten Thije, 2007)

The penalty-polymer model includes penalty contact in combination with a viscous type of friction. The frictional properties are calculated using the shear deformation of a fluid film, present between the two contact surfaces. The frictional properties depend on the contact pressure and slip velocity. This model is suited for modelling the friction between surfaces, lubricated by molten polymers. The total traction vector $\boldsymbol{\tau}$ is calculated as:

$$\boldsymbol{\tau} = \boldsymbol{\tau}_{\mathrm{p}} + \boldsymbol{\tau}_{\mathrm{f}} + \boldsymbol{\tau}_0 \tag{1.18}$$

where $\boldsymbol{\tau}_p$ denotes the contribution of the penalty contact, $\boldsymbol{\tau}_f$ the contribution of the fluid film deformation and $\boldsymbol{\tau}_0$ a constant tangential contribution. The penalty contact is modelled by a penalty formulation:

$$\boldsymbol{\tau}_{\mathbf{p}} = \begin{Bmatrix} 0 \\ 0 \\ \mathrm{p} \end{Bmatrix} \tag{1.19}$$

where the contact pressure p is given by:

$$\mathrm{p} = \mathrm{E_p}.\delta \tag{1.20}$$

with E_p the penalty stiffness and δ the penetration depth. The traction τ_f due to the fluid film deformation is calculated as:

$$\boldsymbol{\tau}_{\mathbf{f}} = \eta.\begin{Bmatrix} \dot{\gamma}_{\mathrm{x}} \\ \dot{\gamma}_{\mathrm{y}} \\ 0 \end{Bmatrix} \tag{1.21}$$

in which $\dot{\gamma}_x$ and $\dot{\gamma}_y$ are the shear rates in the fluid film defined as follows:

$$\begin{Bmatrix} \dot{\gamma}_x \\ \dot{\gamma}_y \end{Bmatrix} = \frac{1}{h}\begin{Bmatrix} v_x \\ v_y \end{Bmatrix} \tag{1.22}$$

where h denotes the thickness of the fluid film and v_x and v_y are the relative slip velocities of the contact surfaces. These are described as:

$$\begin{Bmatrix} v_x \\ v_y \end{Bmatrix} = \frac{1}{\Delta t}\begin{Bmatrix} u_x \\ u_y \end{Bmatrix} \tag{1.23}$$

with Δt the time increment and u_x and u_y the relative incremental displacements of the contact surfaces. The viscosity η of the fluid is given by:

$$\eta = c_p \eta_c \tag{1.24}$$

in which c_p is a function to include the effect of the contact pressure p and is given by:

$$c_p = a\left(p_0 + p\right)^b \tag{1.25}$$

The parameters a, b and c_p are the fitting parameters. The viscosity of the polymer film η_c, is modeled by a cross viscosity model as follows:

$$\eta_c = \frac{\eta_0}{1 + \left(C\dot{\gamma}_q\right)^{(1-n)}} \tag{1.26}$$

with η_0, C and n the fitting parameters and $\dot{\gamma}_q$ the equivalent shear rate:

$$\dot{\gamma}_q = \sqrt{\dot{\gamma}_x^2 + \dot{\gamma}_y^2} \tag{1.27}$$

Some lubricants show a constant level of friction at low slip velocities. A constant tangential traction $\boldsymbol{\tau}_0$ is added to the model to capture this behaviour. The top figure (Figure 1.11) shows the contribution of the two components $\boldsymbol{\tau}_\mathbf{f}$ and $\boldsymbol{\tau}_0$ separately. The bottom figure (Figure 1.11) shows the summed contribution of $\boldsymbol{\tau}_\mathbf{f}$ and $\boldsymbol{\tau}_0$.

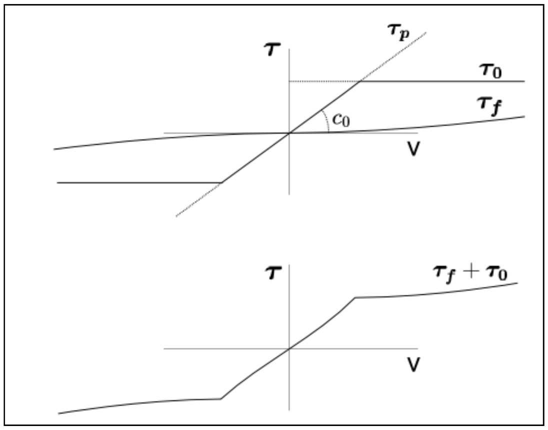

Figure 1.11 Constant tangential contribution

A constant c_0 is introduced to create a well-defined transition when the velocity $\mathbf{v}$ is reversed. This allows the numerical calculations to run smoother. The proportional tangential traction $\boldsymbol{\tau}_{pt}$ equals:

$$\boldsymbol{\tau}_{pt} = c_0 . \begin{Bmatrix} v_x \\ v_y \\ 0 \end{Bmatrix} \tag{1.28}$$

Finally, $\boldsymbol{\tau}_0$ is calculated by scaling $\boldsymbol{\tau}_{pt}$ if its length exceeds the user supplied scalar value $\boldsymbol{\tau}_0$.

$$\boldsymbol{\tau}_0 = \boldsymbol{\tau}_{pt} \ \mathit{if} \ \boldsymbol{\tau}_{pt} \le \boldsymbol{\tau}_0 \tag{1.29}$$

$$\boldsymbol{\tau}_{\mathbf{0}} = \boldsymbol{\tau}_{\mathbf{0}} \cdot \frac{\boldsymbol{\tau}_{pt}}{\left\| \boldsymbol{\tau}_{pt} \right\|} \ \mathit{if}\ \boldsymbol{\tau}_{pt} > \boldsymbol{\tau}_{\mathbf{0}} \tag{1.30}$$

1.4.7 Adhesion model

The adhesion model for the contact interface is used to model the 'tackiness' between surfaces. The normal pressure τn on the contact surface equals:

$$\tau n = -t \tag{1.31}$$

where t denotes the tension that keeps the surfaces together. Trigger distances can be set to activate and deactivate the adhesion model.

CHAPTER 2

RESEARCH STRATEGY

2.1 Research objective

The objective of this research is to study the formability of thermoplastic PPS/CF composite material. Based on experimental results, primary material models and their parameters were investigated for the numerical simulation of the stamp forming process. Then, forming simulations were performed to predict the shape deformations in the stamp forming of PPS/CF composite material and to optimize the mould designs for the forming of diverse geometries, a process which would be very difficult to realize by experimental processes, since the costs of mould designs and fabrication are very high.

2.2 Research strategy

To study the effects of material properties and experimental parameters on the forming results, this research project was divided into three phases, with different forming geometries for each phase as presented in Figure 2.1. These phases progress from a single curvature geometry (phase I) to a double curvature geometry (phase II) and a complex geometry (phase III), which is a real application in airplane structures. In each phase, forming simulations and experiments have been performed for several laminates with different stacking sequences and number of plies, as illustrated in Table 2.1.

Figure 2.2 presents the research strategy. Firstly, forming experiments will be performed for phase I geometry with a four-layer laminate to study the forming process parameters such as blank temperature, mould temperature and forming pressure. Secondly, forming experiments and simulations for phase II geometry with a four-layer laminate will be done. The differences between simulation results and experimental results will be minimized using a simulation-based optimization technique to characterize a subset of material parameters. The optimized material parameters will be validated by comparing the numerical predictions with the experimental results obtained in phase II with a ten-layer laminate and in phase I with a four-layer laminate. Then, a new series of forming simulations will be performed for a real case of mould design in phase III in which many different shapes and laminate stacking sequences will be investigated.

Table 2.1 Laminate setups for three phases

Phase	Stacking sequence	Number of plies	Thickness (mm)
Phase I	(0,90)4	4	1.24
	[(0,90)/(±45) /(0,90)/(±45)/(0,90)]s	10	3.1
Phase II	(0,90)4	4	1.24
	[(0,90)/(±45) /(0,90)/(±45)/(0,90)]s	10	3.1
Phase III	[(0,90)/(±45)/(±45)/(0,90)]s	8	2.48

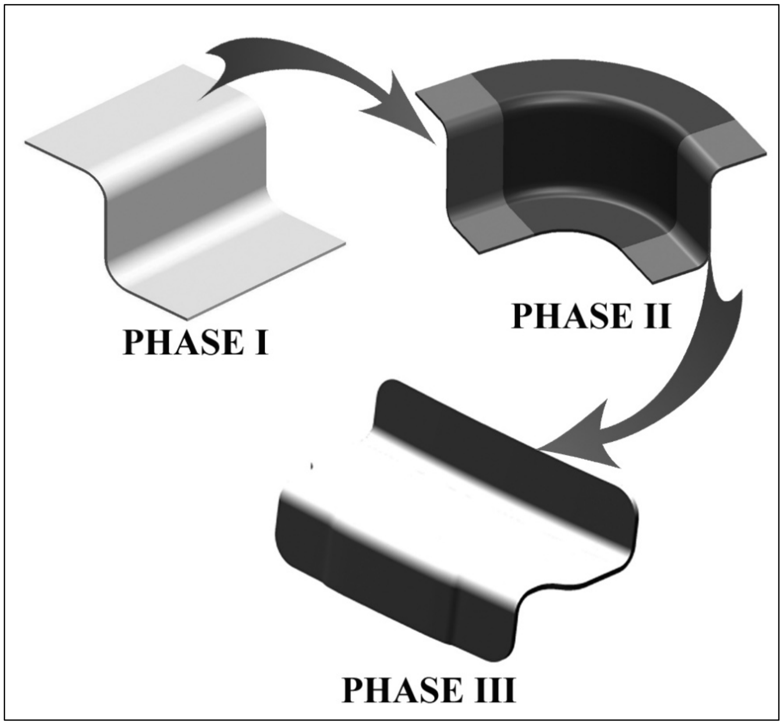

Figure 2.1 Three phases of the project

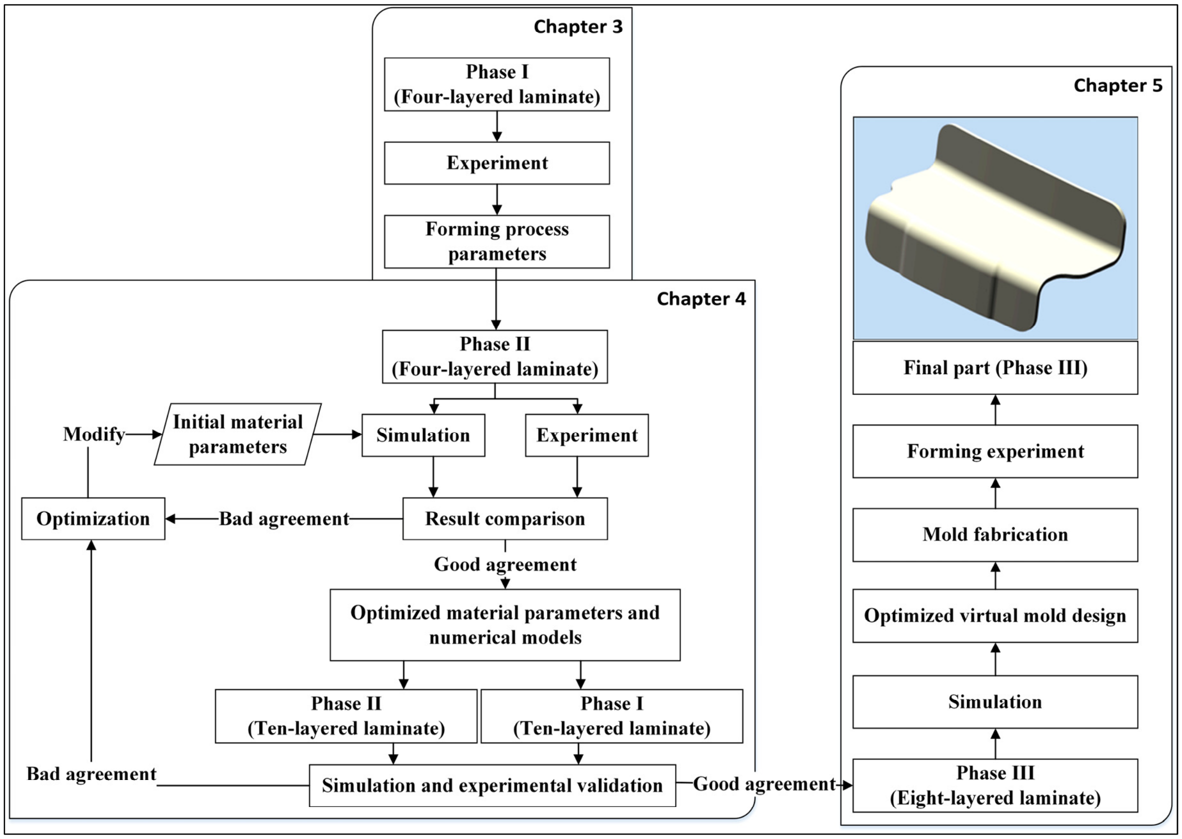
Chapter 3
Phase I
(Four-layered laminate)
Experiment
Forming process parameters
Chapter 4
Phase II
(Four-layered laminate)
Modify
Initial material parameters
Simulation
Experiment
Optimization
Bad agreement
Result comparison
Good agreement
Optimized material parameters and numerical models
Phase II
(Ten-layered laminate)
Phase I
(Ten-layered laminate)
Bad agreement
Simulation and experimental validation
Good agreement
Chapter 5
Final part (Phase III)
Forming experiment
Mold fabrication
Optimized virtual mold design
Simulation
Phase III
(Eight-layered laminate)

Figure 2.2 Research strategy

CHAPTER 3

FORMING EXPERIMENT OF THE SINGLE CURVATURE SHAPE - PHASE I

3.1 Material properties

The base material used is the pre-consolidated carbon fiber-reinforced polyphenylene sulphide (CF/PPS) commercialized by Royal Tencate Corp. It is composed of a polyphenylene sulphide (PPS) matrix reinforced by carbon fiber. The fiber volume fraction (V_f) is 50% and the stacking sequence is $(0, 90)_{4.}$ The thickness of the four-layer laminate is 1.24±0.02 mm. The blank was 315 mm long and 205 mm wide.

3.2 Experimental process

The experimental setup included an infrared oven used as heating unit for the blank. A support frame was used to transfer the blank from the oven to the mould. Moulds were installed on the press and the computer was used to control the forming process. Firstly, the blank was placed onto the Kapton film and centered in the frame. Then the frame was placed in the infrared oven as shown in Figure 3.1. The blank was heated to the temperature of 320 ^{0}C, transferred to the press and placed between two half -moulds. The two half- moulds were also heated to 200 ^{0}C. The mould was then closed and the blank pressurized in order to form the laminate to the mould geometry, as illustrated in Figure 3.2**.** Thereafter, the mould cooling- down process was started and maintained up to the moulding temperature. Finally, the mould was opened and the part was removed. The pressing, holding and demoulding processes in the forming station were fully programmed through LabVIEW control system. The experimental parameters are presented in Table 3.1 and the formed part is shown in Figure 3.3. The part surfaces are very smooth without any wrinkles or unwanted distortions.

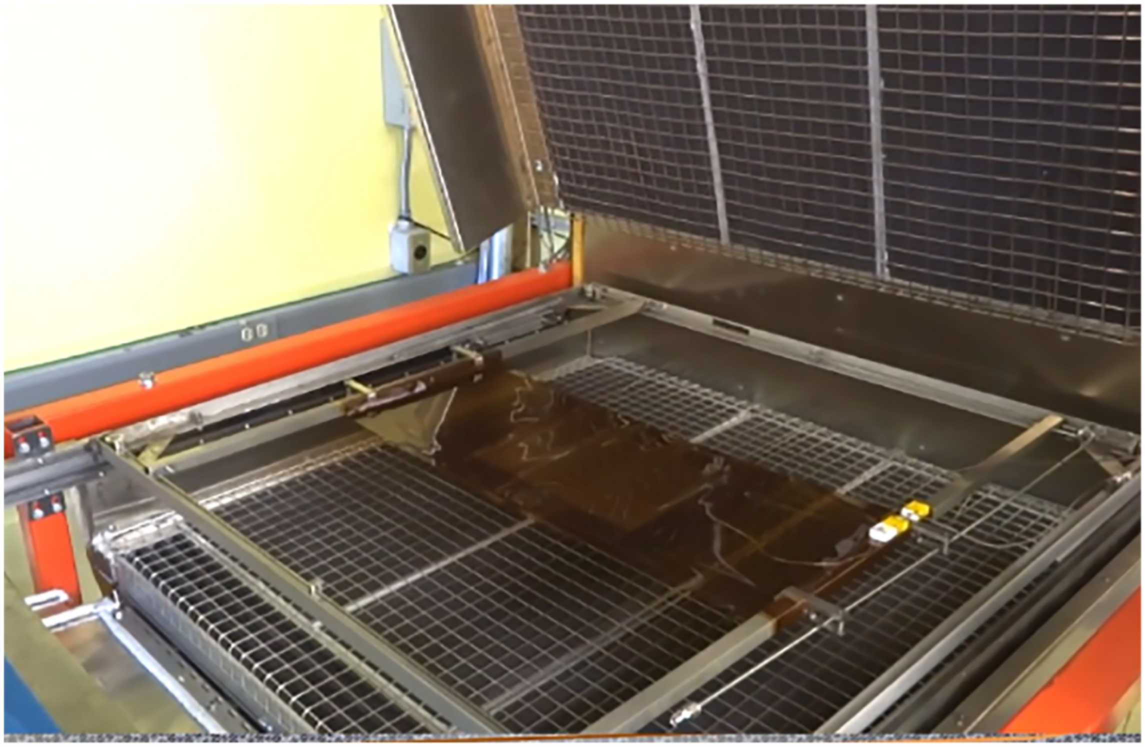

Figure 3.1 The blank was placed onto the Kapton film.

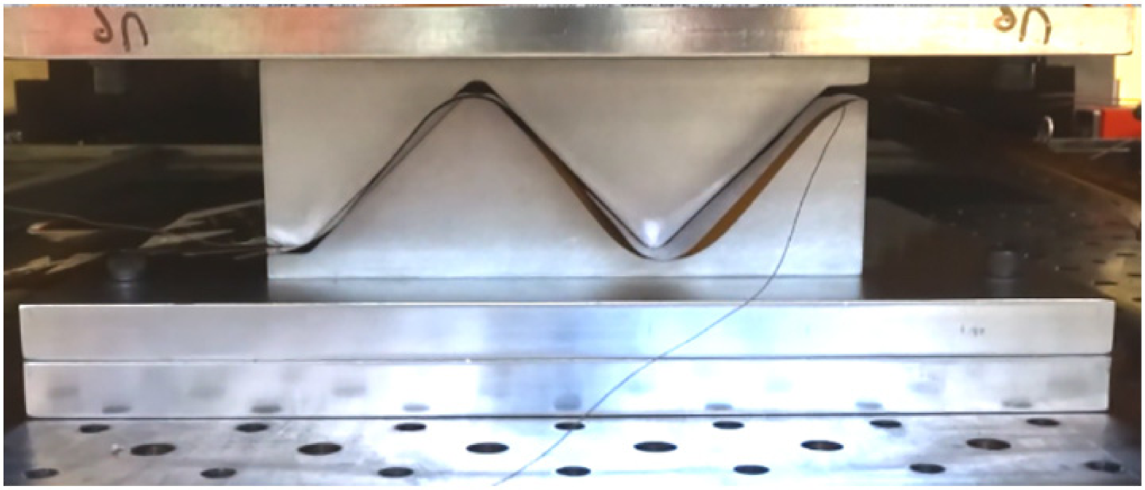

Figure 3.2 The mould was fully closed

Table 3.1 Experimental processing parameters for forming of phase I

Blank temperature (°C)	Mould temperature (°C)	Holding time (min)	Stamping force (Tons force)
320	200	2	20

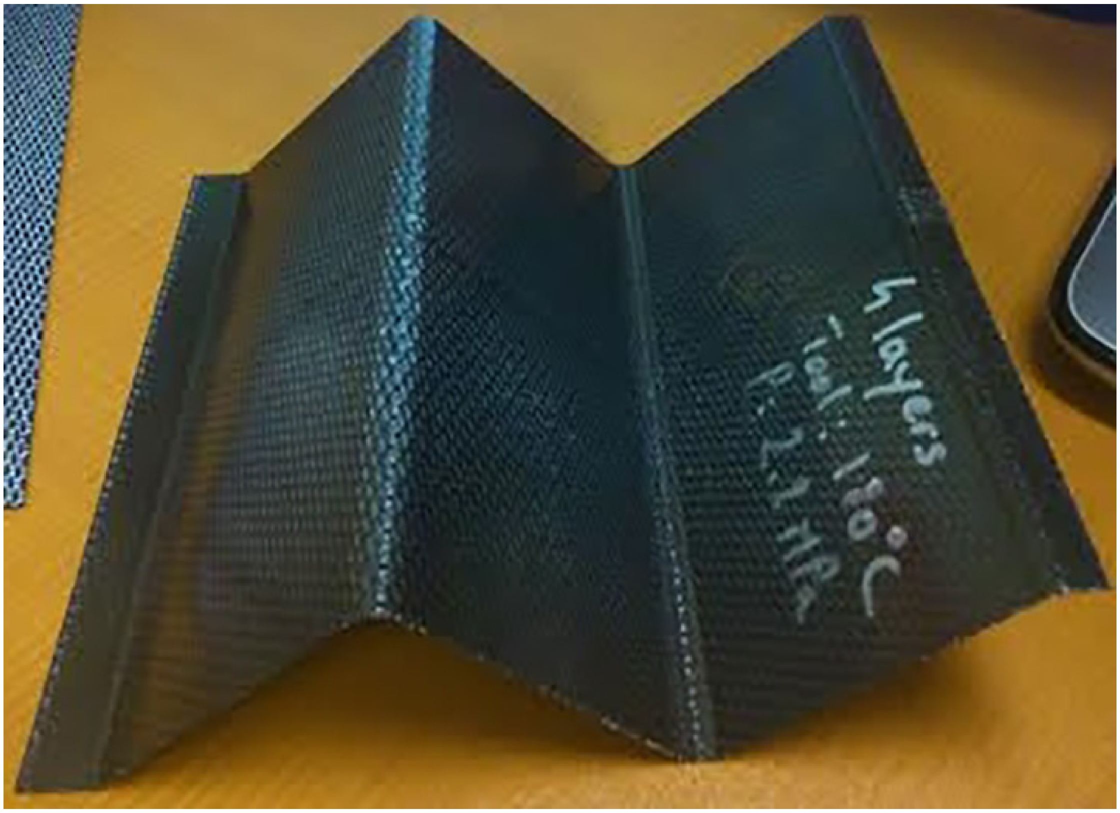
4layers
Tool: 180°C
P: 2.1MPa

Figure 3.3 The formed part

CHAPTER 4

INVERSE CHARACTERIZATION OF MATERIAL PROPERTIES FOR SIMULATION OF STAMP-FORMING OF MULTI-LAYER THERMOPLASTIC PPS/CF COMPOSITES[*]

Abstract

In this paper, the stamp forming of four-layer laminate and ten-layer laminate of PPS/CF composites has been well researched in both experiment and simulation. The effects of numerical model combinations and material properties on forming predictions have been studied. A good numerical model combination for stamp-forming prediction has been investigated. The optimized material properties for forming simulation of multi-layer laminate of PPS/CF composites have been identified using multi-objective optimization technique that minimizes the difference between experimental and numerical results in term of thickness, shear-angle and wrinkle distributions. Intra-ply shear, bending behaviours and the contact logic between the individual plies and between tool-ply have been modelled in these simulations. The predicted results agreed well with the experimental results. The optimized material properties and the studied numerical model combination have been successfully used to predict the forming process for several geometries and different laminate stacking sequences.

Keywords

Composites, modelling, thermoplastic, optimization, stamp-forming, simulation

4.1 Introduction

There are considerable applications of fiber-reinforced thermoplastic composite (FRTPC) materials for aerospace and automotive components. There are many advantageous characteristics of thermoplastic composites compared to thermoset composites. For instance, thermoplastic composite components may be thermoformed with short cycle times. They are highly recyclable and they could be used for remoulding and reshaping. Thermoplastic composites have excellent mechanical properties, high temperature resistance, high impact resistance and good chemical resistance. Thermoplastic composites are also lighter and easier to colour than thermoset materials. These are just some to be named here, but not all. Thanks to their advantages, thermoplastic composites are gradually replacing thermoset composites for laminate fabrication particularly for high volume applications.

---

[*] Reproduced from: Hong-Den Nguyen, Xuan-Tan Pham and Martin Deshaies. Inverse characterization of material properties for modelling of stamp-forming of multi-layered thermoplastic PPS/CF composite. Prepared for *Journal of Reinforced Plastics and Composites*, **2015.**

However, there are still various difficulties in forming of thermoplastic composite materials. The forming must be performed at elevated temperature and high pressure. High slippages between layers may appear at high temperature due to the change of friction between tool-ply and between ply-ply (Nguyen *et al.*, 2015). Thermoplastic composite forming may create wrinkles and thickness variation in formed parts. The practical difficulties of forming successfully thermoplastic composite components have led to a requirement for understanding the mechanical properties of FRTPC sheets and for the development of computational techniques for process simulations based on these properties. While experimental methods may be used to understand the forming of these materials, numerical simulations offer an efficient and rapid tool to study the mechanism of deformation of FRTPC sheets.

For numerical simulations, it is indispensable to understand the deformation mechanisms of materials during the forming process, to identify the numerical models that could take into account these deformation mechanisms and to determine the material parameters for these numerical models. The deformation mechanisms of thermoplastic composites have been studied in several research papers (Haanappel, 2013; Long, 2007; Ten Thije, 2007). Some mechanical behaviours such as bending behaviour, intra-ply shear and axial loading deformation have been studied as primary deformation mechanisms. Many numerical models have been developed and published during last few years. However, it has not been yet determined how to combine these primary numerical models to better predict a forming process, and this will be the main object of the current research in which the stamp-forming of thermoplastic PPS/ Carbon fiber composite (PPS/CF) is studied. The PPS/CF composite is one of the most frequently used thermoplastic composite materials for aircraft structures. The properties of this material have been investigated in several researches (Díez-Pascual *et al.*, 2012; Liu *et al.*, 2015). However, it is sometimes quite hard to get good values of material parameters just by characterization tests since the stamp-forming process is at high temperature and high pressure. The friction properties are not significant in single-layer forming simulations (Hamila *et al.*, 2013; Hussein *et al.*, 2013), but they are very important in multi-layer forming simulations. It is observed that the friction between tool-ply or between ply-ply is not easy to be measured at this forming condition. On the one hand, this research will study the effect of the material parameters to the forming prediction and identify material parameters using simulation-based optimization technique based on experimental results. On the other hand, forming predictions of different geometries and different laminate stacking sequences for PPS/CF composites using the optimized material properties and the best choice of material model combination will be validated with experimental forming results in terms of wrinkles apparition, thickness distribution and fiber shear angles.

4.2 Forming experiment

Experiments were performed using a stamp-forming system at National Research Council Canada - Aerospace as shown in Figure 4.1. The composite material used in these experiments is the pre-consolidated carbon fiber-reinforced polyphenylene sulphide (CF/PPS) commercialized by Royal Tencate Corp. It is composed of a polyphenylene sulphide (PPS) matrix and carbon fiber fabrics. The fiber volume fraction (V_f) is 50% and the layer thickness is 0.31 mm. The blank was installed in the oven using a frame as shown in Figure 4.2 and it was heated to 320^{o}C. Once the prescribed temperature was reached, the blank was transferred from the oven to the stamp-forming machine and placed between the two half moulds. The mould was then closed and the blank was pressurized with 35 tons-force in order to form the laminate to the mould geometry. Figure 4.3 presents an example of formed part from this system.

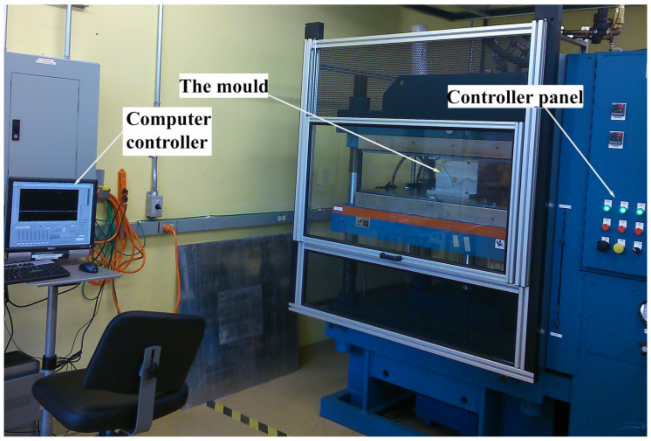
The mould
Controller panel
Computer controller

Figure 4.1 Stamp forming system

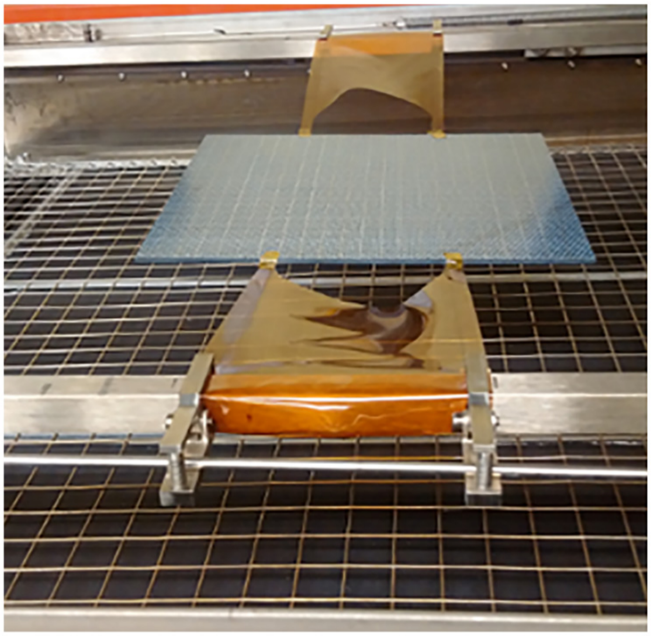

Figure 4.2 Blank is in the oven

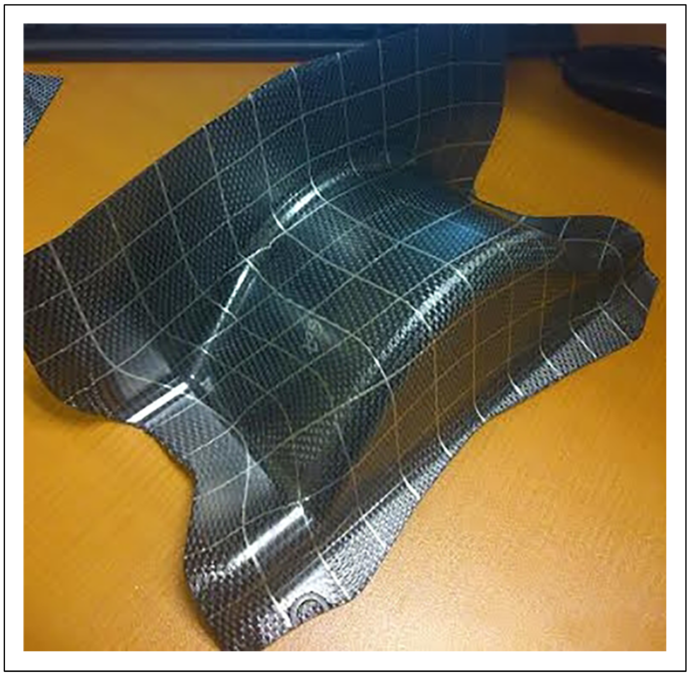

Figure 4.3 The formed part

4.3 Deformation mechanisms

The deformation mechanisms of PPS/CF composite material can be divided into three main categories: in-plan, inter-ply and out-of-plane mechanisms as depicted in Figure 4.4. The in-plan behaviour includes the axial loading deformation and the intra-ply shear deformation. The intra-ply shear is usually considered as a primary deformation mechanism for aligned fiber-based materials. It includes the longitudinal intra-ply shearing which is the sliding of parallel tows within a composite ply, and the transverse intra-ply shearing which is the rotation of tows at their crossovers (Long, 2007). It is observed that the loading along the fiber axis results in very large forces and low maximum strains in comparison to intra-ply shear. The out-of-plan behaviour includes the bending and the compaction deformation. During the forming process, the friction between the material and forming tools plays an important role in the transfer of loads to the material. In multi-layer forming processes, the friction between individual layers of material is also of importance. The values of friction at ply-tool and ply-ply interfaces are a key factor to simulate accurately the forming process.

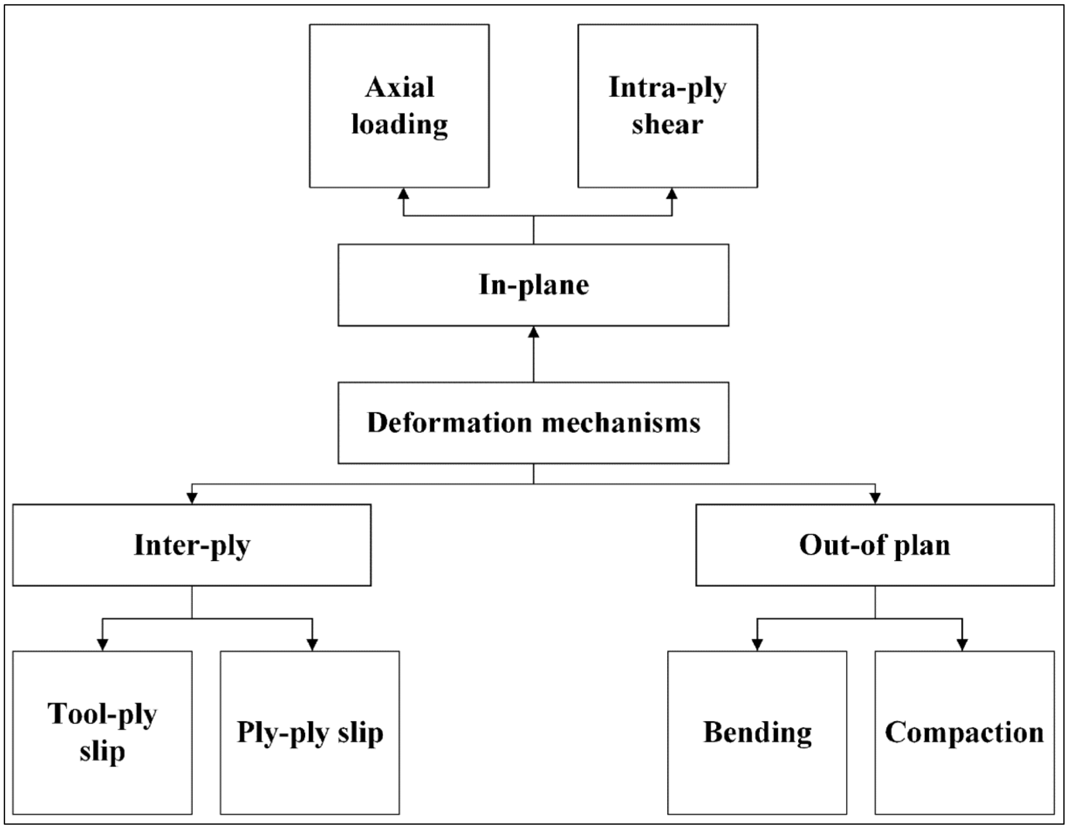
Axial loading
Intra-ply shear
In-plane
Deformation mechanisms
Inter-ply
Out-of plan
Tool-ply slip
Ply-ply slip
Bending
Compaction

Figure 4.4 Deformation mechanisms

4.4 The effects of numerical model combinations on forming predictions

4.4.1 Numerical models and material properties

The simulations with two different material model combinations were performed to study the effects of the material model combinations on forming predictions in order to determine the best choice of numerical model combination for future forming predictions. Table 4.1 shows the numerical models that could take into account the deformation mechanisms of PPS/CF composites. The Isotropic Elastic model (Annin *et al.*, 2015) is used to model the ply bending. The tool-ply and ply-ply contact interactions are modelled by the Penalty-Polymer model (Ten Thije, 2007) and the Adhesion model (He *et al.*, 2013). The difference between two options is the choice of material models used for modelling the in-plane behaviour of the plies as presented in Table 4.1. In option A, the in-plane behaviour was modelled by an assembly of three models: the Fabric Reinforced Viscous Fluid (FRVF) model (Spencer, 2000), the Newton fluid model and the elastic fiber model. Meanwhile, the elastic fiber model (Jones, 1999), the Mooney Rivlin model (Eriksson *et al.*, 2014) and the Cross Viscosity model (Cross, 1965) were used for the in-plane behaviour in the option B. The material characterization tests to identify the material parameters of PPS/CF composites have been carried out in several researches. The current study focused only on the way to find out the best choice of the numerical model combination and to determined material properties through an advanced multi-objective optimization technique based on the initial material properties collected from the literature (Díez-Pascual *et al.*, 2012; Haanappel, 2013; Ten Thije, 2007; Ten Thije *et al.*, 2011; Ten Thije *et al.*, 2007) as shown in Table 4.2.

Table 4.1 Numerical models

Deformation	Description	Option A	Option B
In-plane	Axial loading deformation	Elastic fiber	Elastic fiber
	Intra-ply shear deformation	RFVF	Mooney Rivlin
		Newton fluid	Cross Viscosity
Out-of-plan	Bending and compaction	Isotropic Elastic	Isotropic Elastic
Inter-ply	Tool-ply slip	Penalty-polymer	Penalty-polymer
	Ply-ply slip	Adhesion	Adhesion

Table 4.2 Material properties

Numerical model	Material parameter	Description	Unit	Value
Isotropic Elastic	E	Young’s module	[MPa]	15000
	υ	Poisson’s ratio		0.33
Cross Viscosity	η_o	viscosity at low shear rate	[MPa.s]	0.682
	η_∞	viscosity at high shear rate	[MPa.s]	0
Elastic fiber	E_f	Young's modulus of the fiber	[MPa]	70000
	ρ	density of the material	[kg/mm^3]	1350x10^{-9}
Mooney-Rivlin	c_{10}	material constant	[MPa]	0.165
	c_{01}	material constant	[MPa]	0.00524
Newton fluid	ρ	density of the material	[kg/mm^3]	1350x10^{-9}
	η	viscosity	[MPa.s]	0.1
Penalty-polymer	h	film thickness	[mm]	0.02
	η_0	viscosity	[MPa.s]	750x10^{-6}
	E_p	penalty stiffness		1
Adhesion	t	adhesion	[MPa]	0.1

4.4.2 Simulation setup

Figure 4.5 illustrates the stamp-forming simulation setup. Both the mould and the punch were modelled as rigid surfaces with around 20000 triangular elements for each. Meanwhile, each material ply was modelled with 12000 triangular elements. The blank was laminated by four layers of 285 mm long and 241 mm wide with the stacking sequence $(0,90)_4$. The forming process was simulated by moving the punch downward. Firstly, the punch was moved very quickly to the laminate surface. Secondly, the punch was moved downward slowly at the speed of 20 mm/s until the gap between the punch surface and the mould surface was equal to the laminate thickness.

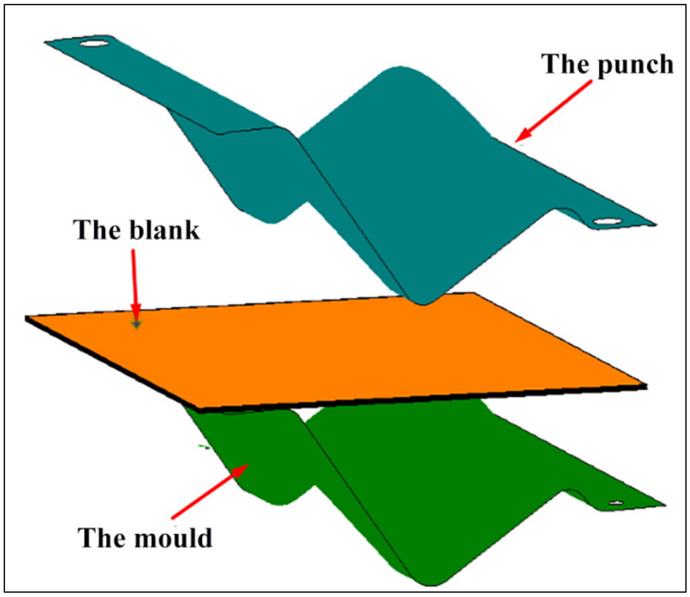

Figure 4.5 Simulation setup

4.4.3 Predicted result and experimental validation

Forming simulations of multi-layer PPS/CF composites were successfully performed. The predicted results in terms of shape deformation and wrinkle distribution agreed very well with the experimental results. There was no wrinkle in the predicted and experimental results as shown in Figure 4.6. The formed parts were cut out to measure the thickness using a digital calliper. Thickness and shear-angle were measured along a line as depicted in Figure 4.7. Fiber orientations were evaluated based on shear-angle values which are the difference between the initial angles and the formed angles between two fiber families. The experimental shear-angles were evaluated based on the initial angles and formed angles between horizontal lines and vertical lines which were drawn onto the blank as illustrated in Figure 4.8.

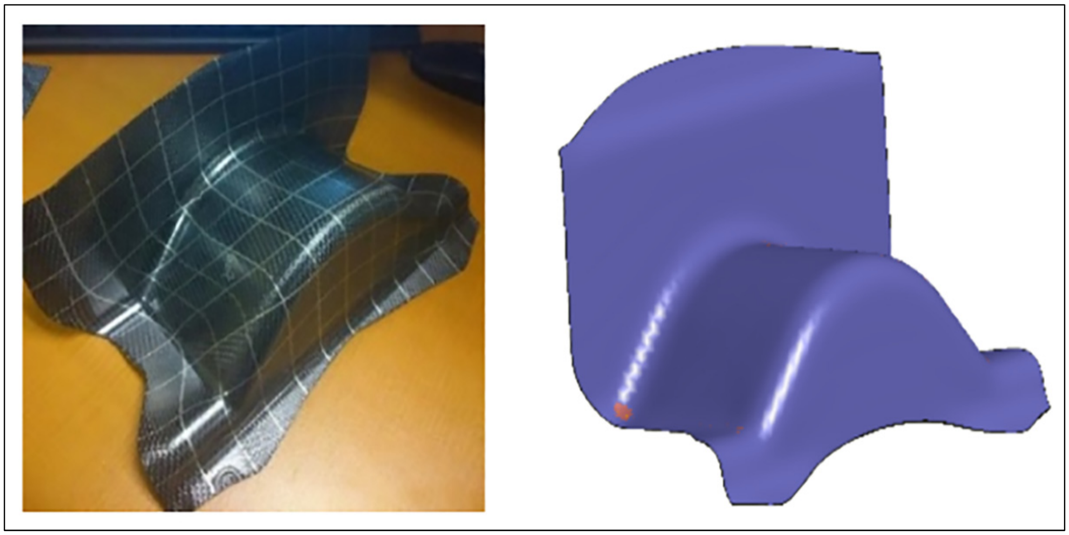

Figure 4.6 General deformation

The thickness and shear-angle distributions are presented in Figure 4.9 and Figure 4.10, respectively. The predicted results in option B showed a better agreement with the experimental results than that in option A. The initial thickness was 1.24 mm. It was observed that the thickness increased everywhere in the formed part after the deformation. The highest experimental thickness value was 1.36 mm. It increased more than 9.5% in comparison to the initial thickness. The maximum shear-angle measured from the formed part as high as 26 degrees. It was remarked that the choice of numerical models and the combination between them have very high effects to the predicted results. The material model combination that gave the best prediction of PPS/CF composite forming was found as shown in Table 4.1 (Option B).

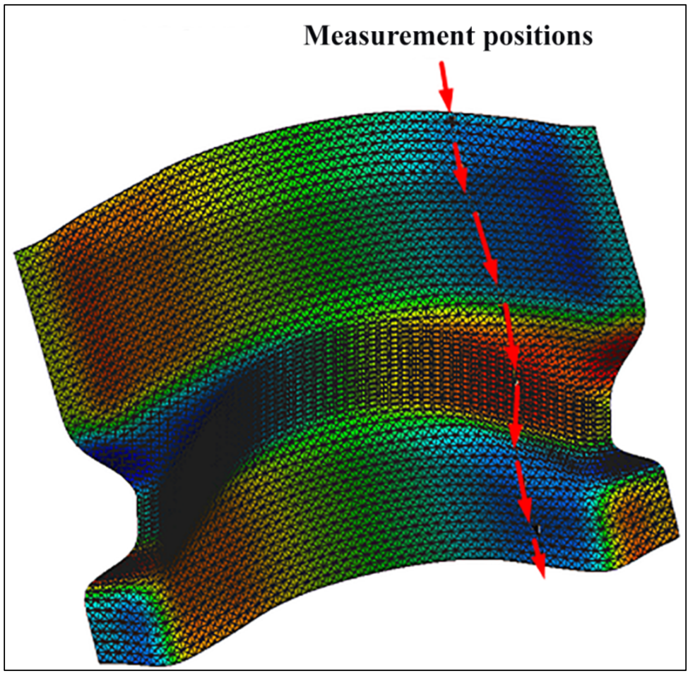
Measurement positions

Figure 4.7 Measurement positions

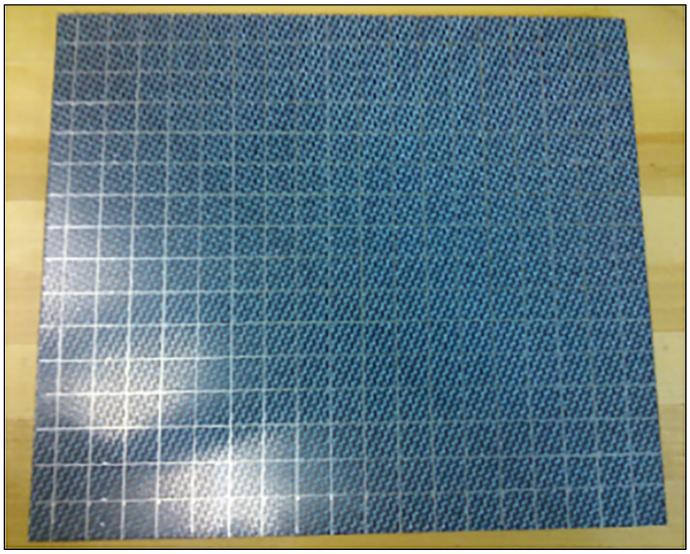

Figure 4.8 Draw lines on the blank

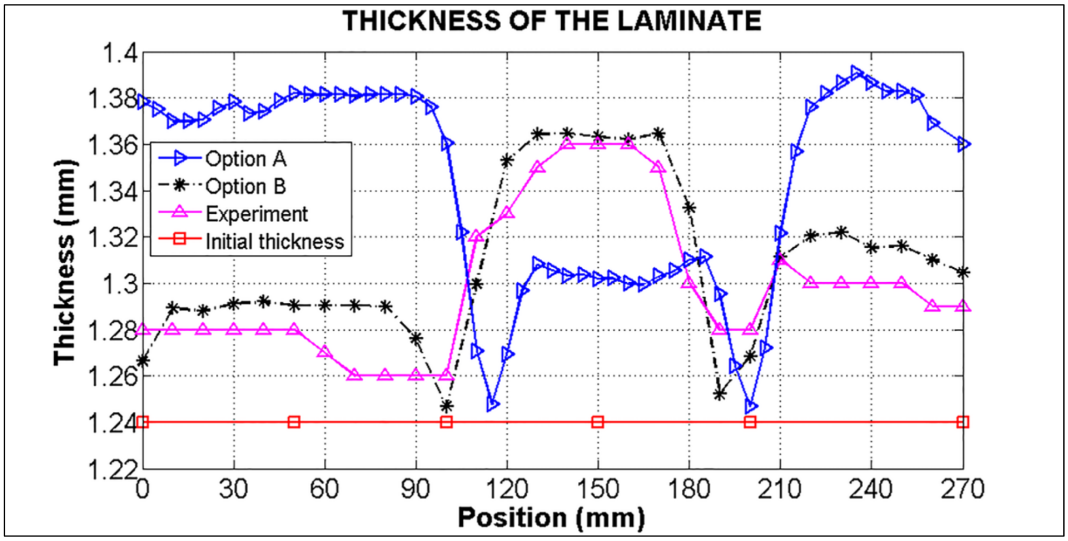

Figure 4.9 Thickness distribution

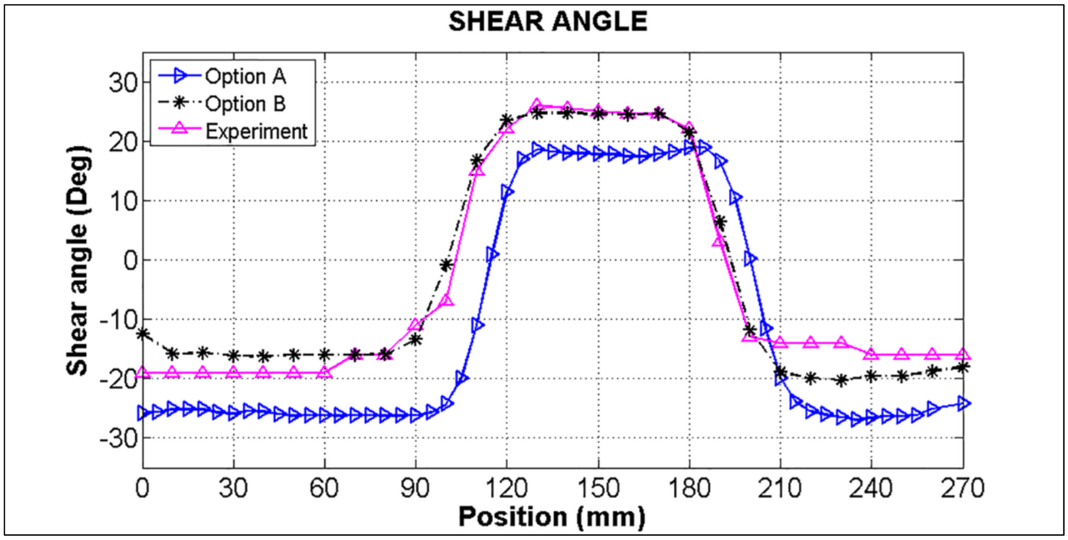

Figure 4.10 Shear-angle distribution

4.5 Inverse material characterization procedure and the effects of material properties on forming predictions

4.5.1 Simulation-based inverse characterization procedure

The best combination of numerical models found in the previous paragraph corresponded to option B in which the primary numerical models and the material parameters were shown in Table 4.1 and Table 4.2, respectively. It is noted that more than thirty material parameters are required in a numerical simulation with Aniform. Some of them were obtained by material characterization tests and the others were found in the literature such as density, Young's modulus, Poisson's ratio of this material. It is quite hard if not impossible to get the accurate values for some parameters from material characterization tests, for example, the tool-ply friction, the ply-ply friction or the penalty stiffness between plies for numerical models. In this study, an inverse characterization method using simulation-based optimization technique was employed in order to determine a set of parameters which minimizes the discrepancy between the experimental and predicted results in term of thickness and shear-angle variation. The inverse material characterization procedure is presented in Figure 4.11. In this simulation-based inverse characterization method, the initial values for the optimization procedure are the results of the numerical simulation performed with the initial materials parameters shown in Table 4.2 which are correspondingly for the numerical models of option B as mentioned above. The predicted results are compared with the experimental results through a multi-objective function (Equation 3) in term of thickness and shear-angle values evaluated at a number of positions on the formed part as the following.

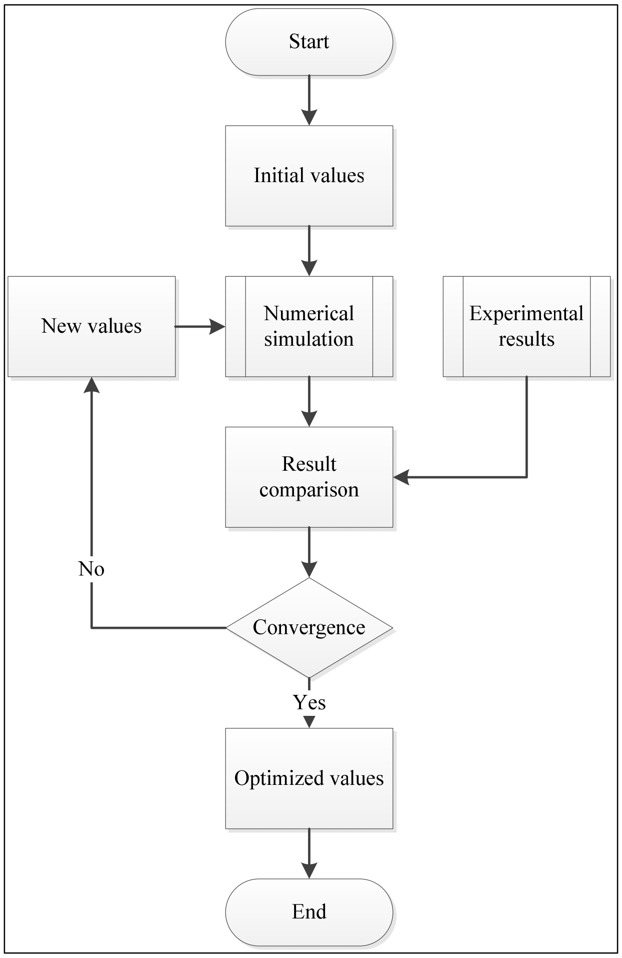
Start
Initial values
New values
Numerical simulation
Experimental results
Result comparison
No
Convergence
Yes
Optimized values
End

Figure 4.11 Simulation-based inverse characterization procedure

The difference between the predicted thickness and the experimental thickness is evaluated by the residual sum of squares:

$$F(x) = \sum_{j=1}^{n} (x_j^{\text{sim}} - x_j^{\text{exp}})^2 \tag{4.1}$$

where x_j^{sim} and x_j^{exp} are the predicted and experimental thickness values at point j and n is the total number of points used for the evaluation. Similarly, the difference between the predicted shear-angles and the experimental shear-angle is expressed by:

$$F(\mathrm{y}) = \sum_{j=1}^{n} (y_j^{\mathrm{sim}} - y_j^{\mathrm{exp}})^2 \tag{4.2}$$

where y_j^{sim} and y_j^{exp} are the predicted and experimental shear-angle values at point j. The multi-objective function is then defined from Equations 1 and 2 as follows:

$$F(\mathrm{x}, \mathrm{y}) = F(\mathrm{x}) + F(\mathrm{y}) \tag{4.3}$$

The optimization loop is repeated to minimize this objective function until the convergence criteria are satisfied for that an optimized set of materials parameters are finally identified.

4.5.2 Inverse characterization result analysis

It was observed in the previous paragraph that the numerical results (with option B) using the initial material parameters were slightly different from the experimental results as shown in Figure 4.9 and Figure 4.10. It is due to the fact that it is quite hard to get good values just by material characterization tests for a group of seven material parameters as presented in Table 4.3. The values of these parameters were obtained by inverse characterization. Each parameter is a continuous variable and bounded by minimum and maximum values.

Table 4.3 Material parameters for optimization

Parameter	Description	Unit	Initial	Minimum	Maximum
Ep_1	penalty stiffness tool-blank		1	0.3	1.5
Ep_2	penalty stiffness ply-ply		1	0.3	1.5
η_{01}	tool-ply viscosity	[MPa.s]	$750\text{x}10^{-6}$	0.0001	0.0009
η_{02}	ply-ply viscosity	[MPa.s]	$750\text{x}10^{-6}$	0.0001	0.0009
c_{10}	material constant	[MPa]	0.165	0.1	0.25
η_{03}	viscosity of Cross Viscosity model	[MPa.s]	0.682	0.1	0.9
t	adhesion	[MPa]	0.1	0.05	0.3

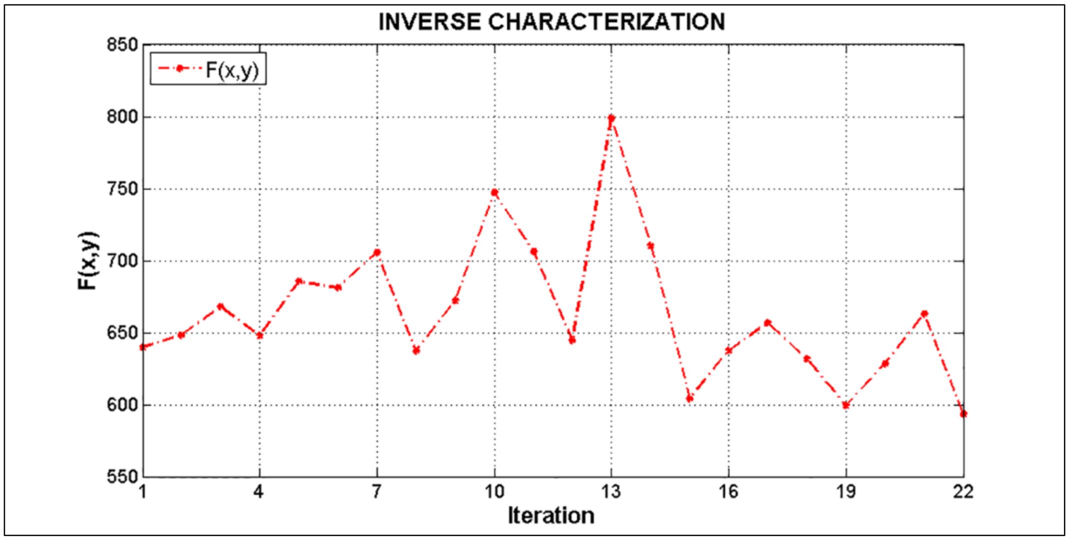

Figure 4.12 Optimization iteration history plot for $F(x,y)$

Thickness and shear-angle were measured along a line as depicted in Figure 4.7. The variation of the objective function during the optimization process is presented in Figure 4.12. It was observed that the optimization process was successfully completed after twenty-two iterations using the Adaptive Response Surface Method (ARSM) in the Altair Hyper-Study software. The optimized material parameters obtained at the 22th iteration are shown in Table 4.4 for that the thickness and shear-angle variations between the experimental results and the predicted results were minimized. Figure 4.13 and Figure 4.15 present respectively the comparison of the thickness and shear-angle values obtained from the initial set of parameters (1st iteration), the best set (22th iteration), the worst set (13th iteration) together with the experimental results. The differences between the experimental values and the predicted values are illustrated in Figure 4.14 and Figure 4.16. The maximum thickness difference between the predicted thickness and the experimental thickness was only 0.03 mm which is in the range of the manufacturing tolerances as high as 0.03 mm or measurement tolerances up to 0.02 mm. It was observed that the maximum shear angle difference was 7 degrees at the border of the part where the experimental part was affected by the delamination of the laminate and the slippages between plies. Since practically it is not easy to measure the fiber orientations of the formed part, the shear angle measurement tolerances may be as high as 5 degrees in these locations.

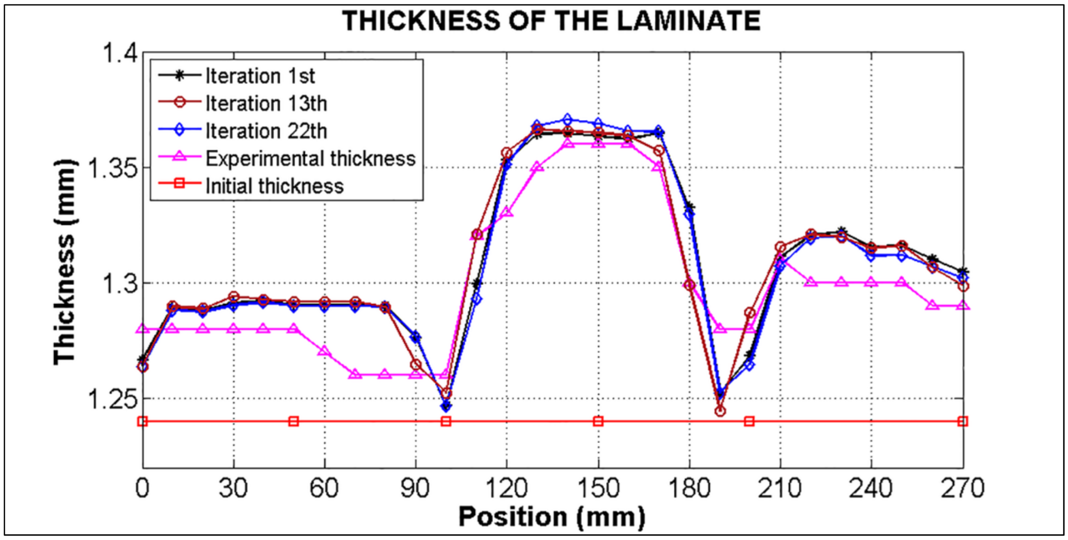

Figure 4.13 Thickness comparison between iterations

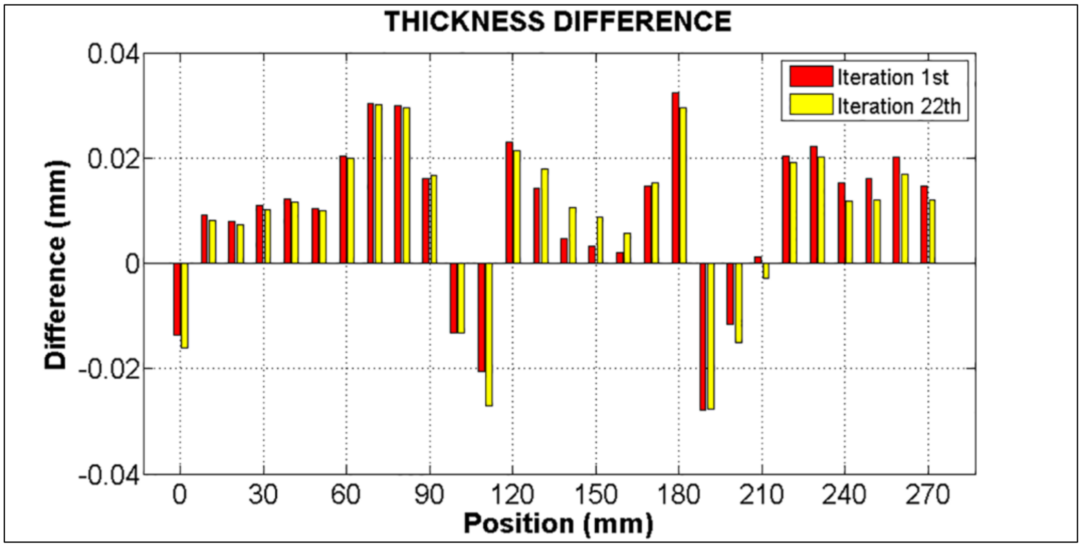

Figure 4.14 Thickness difference between the predicted results and the experimental results

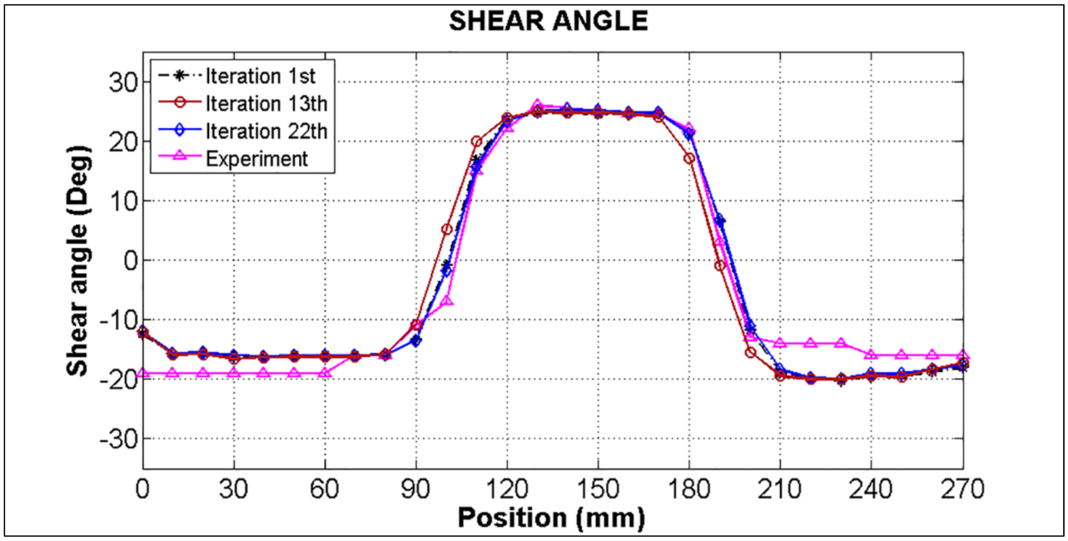

Figure 4.15 Shear angle comparison between iterations

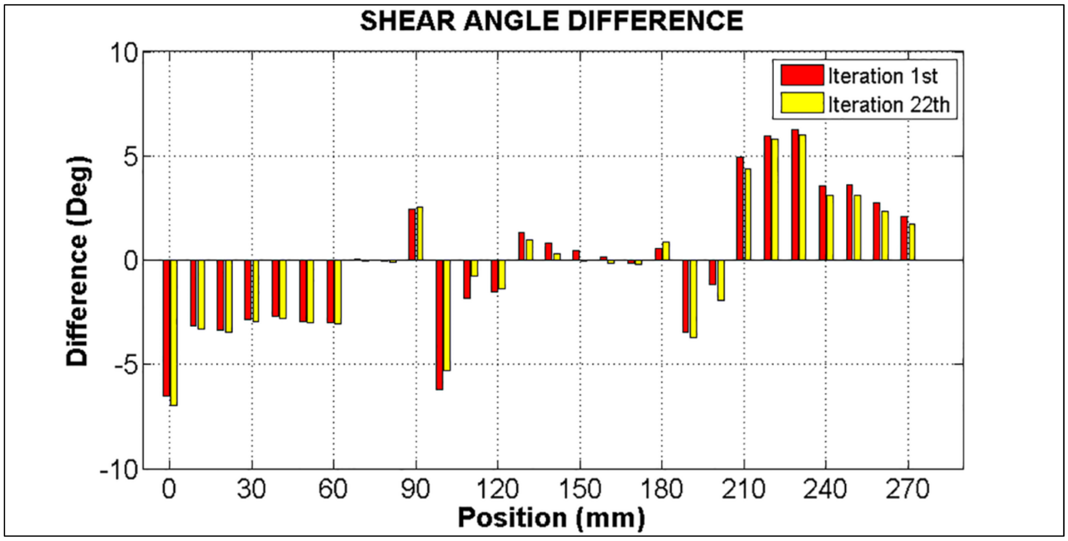

Figure 4.16 Shear angle difference between the predicted results and the experimental results

Table 4.4 Optimization results

Iteration	Ep_1	Ep_2	η_{01}	η_{02}	c_{10}	η_{03}	t	$F(x)$	$F(y)$	$F(xy)$
1	1.0	1.0	$75 \cdot 10^{-5}$	$75 \cdot 10^{-5}$	0.165	0.682	0.10	0.0088	639.84	639.85
22	0.9	0.787	0.0009	0.0005	0.190	0.674	0.15	0.0087	593.63	593.64

To evaluate how well the predicted thickness values fit the experimental thickness values, the coefficient of determination, denoted by R_x^2, is calculated as follows:

$$R_x^2 = 1 - \frac{F(x)}{F(x)_{tot}} \tag{4.4}$$

where F(x) is the residual sum of squares which was calculated by Equation (1) and $F(x)_{tot}$ is the total sum of squares defined by the following expression:

$$F(x)_{tot} = \sum_{j=1}^{n} (x_j^{\text{sim}} - \overline{x_j^{\text{exp}}})^2 \tag{4.5}$$

in which x_j^{sim} is the predicted thickness value at node j and $\overline{x_j^{\text{exp}}}$ denotes the mean of the experimental thickness values:

$$\overline{x_j^{\text{exp}}} = \frac{1}{n} \sum_{1}^{n} x_j^{\text{exp}} \tag{4.6}$$

The coefficient of determination R_x^2 was calculated at two iterations and was presented in Table 4.5. The coefficient of determination increased from 0.750 to 0.767 at the end of the optimization. It means that a better agreement in average was found between the predicted and experimental data by the inverse characterization technique. Similarly, the coefficient of determination for evaluating the shear angle distribution was presented in Table 4.6 where $F(y)$ the residual sum of squares which was calculated by equation (2), $F(y)_{tot}$ the total sum of squares and R_y^2 the coefficient of determination in case of shear angle evaluation. It was observed that the coefficient of determinations R_y^2 was very close to 1. If the coefficient of determinations is equal to 1, it means that there is no difference between the experimental values and the predicted values. However, there are always the manufacturing tolerances, the measurement tolerances or the limitation of the computational modelling.

Table 4.5 Coefficient of determination for evaluating the thickness distribution

Iteration	$F(x)$	$F(x)_{tot}$	R_x^2
1	0.0088	0.0350	0.750
22	0.0087	0.0371	0.767

Table 4.6 Coefficient of determination for evaluating the shear angle distribution

Iteration	$F(y)$	$F(y)_{tot}$	R_y^2
1	639.8	9103.7	0.930
22	593.6	9013.9	0.934

4.6 Validation of optimized material properties and numerical models in term of wrinkle distribution.

The optimized material parameters were found in the previous paragraph as shown in Table 4.4. However, these data need to be validated again to make sure that they could be used for different geometries and different laminate stacking sequences to predict the quality of formed parts particularly the apparition of wrinkles. Two new cases of stamp-forming were performed. The first one was with a new mould design for a ten-layer laminate with the stacking sequence $[(0, 90)/ (\pm 45) / (0, 90)/ (\pm 45)/ (0, 90)]_s$ and the second one was with a new mould design for a four-layer laminate. A good agreement was found between the experimental and predicted results in term of wrinkle distribution as shown in Figure 4.17 and Figure 4.18 respectively for the ten-layer part and the four-layer part. This demonstrated that the optimized material parameters for the selected numerical model combination (option B) are good enough and can be used for general cases of forming of PPS/CF composites.

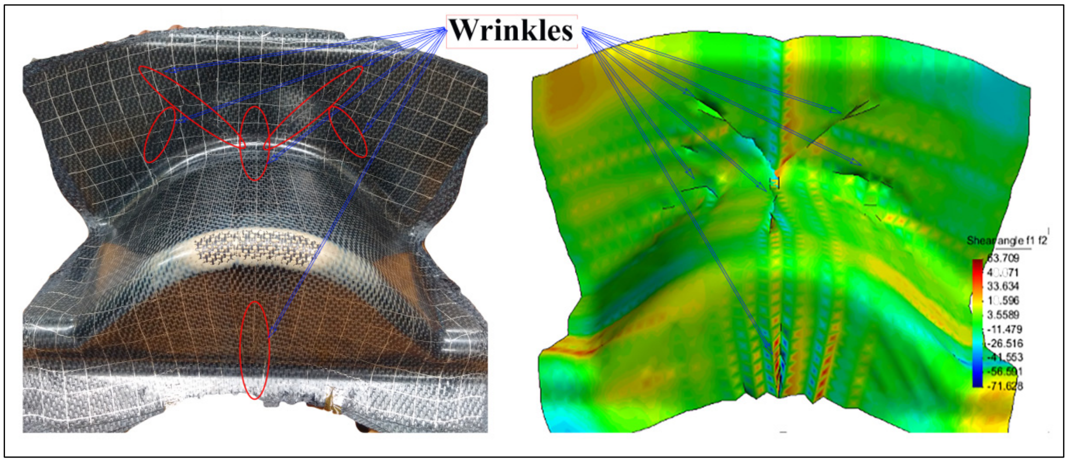
Wrinkles
Shear angle f1 f2
63.709
33.634
3.5589
-11.479
-26.516
-41.553
-56.591
-71.628

Figure 4.17 Wrinkle comparison between the experimental and predicted results of the ten-layer part

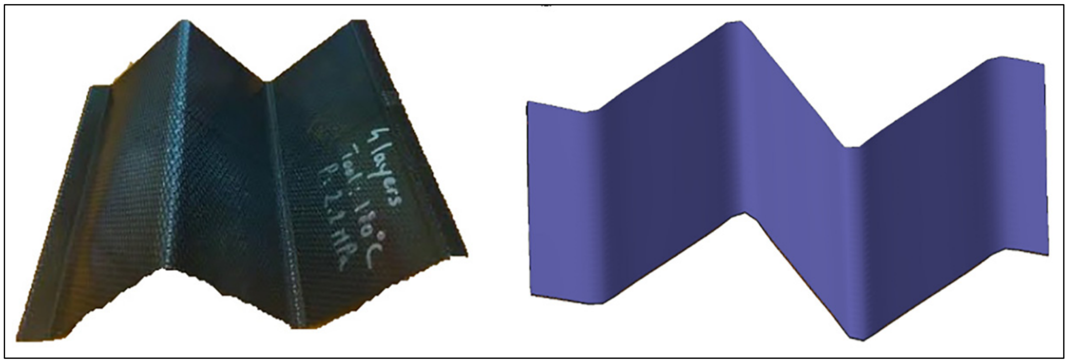
4 layers
Tool: 180°C
P: 2.2 MPa

Figure 4.18 Wrinkle comparison between the experimental and predicted results of the four-layer part

4.7 Conclusions

The results in this study showed that the stamp-forming simulations of multi-layer PPS/CF composites were successfully performed to predict the quality of formed parts in terms of shape deformation, fiber orientations and thickness distribution. Very good agreements between predicted and experimental results were found in this work. Especially, the prediction of wrinkles was well validated with the experimental results for both stamp-forming of the ten-layer laminate and the four-layer laminate. It was observed that the choice of primary numerical model combination for the modelling of deformation mechanisms was a key factor for the success of the numerical simulations. It was demonstrated that the simulation-based optimization technique for inverse characterization is an excellent method to determine material parameters particularly when it is very hard to obtain parameters from characterization tests. This method is very promising for the future work when dealing with different geometries and laminate stacking sequences.

CHAPTER 5

SIMULATION-ASSISTED MOULD DESIGN FOR THE FORMING OF PPS/CF COMPOSITE MATERIALS

5.1 Mould design for the stamp forming (Phase II) with the ten-layer laminate*

5.1.1 Virtual mould design with numerical parametric study

The forming of the ten-layer laminate was performed in both experiments and numerical simulations. The preliminary results shown in Figure 4.17 of Chapter 4 exhibited high shear-angle values and wrinkles in the formed part. A new mould design is required for the forming of the ten-layer laminates to avoid wrinkles. A numerical parametric study with two parameters, the forming angle β and the angle α, as shown in Figure 5.1 was performed to optimize the mould design. Several virtual moulds with different dimensions were suggested in Table 5.1.

Table 5.1 Virtual mould dimensions

Mould name	A	B	C	D	E	F
α	45°	56°	74°	82°	76°	90°
β	33°	35°	33°	52°	55°	57°

---

* Reproduced from: Nguyen, H. D., Deshaies, M. & Pham, X. T. Simulation-assisted mould design for the forming of thermoplastic PPS/CF composites. CASI-GARDN AERO Conference (AERO 2015) Montreal, Canada.

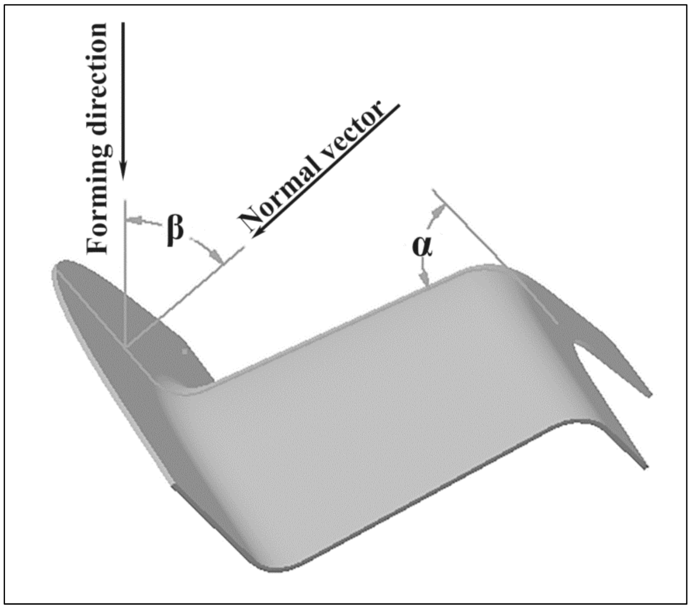

Figure 5.1 Mould geometry

It was observed that the fiber shear angle increases with α and β as shown in Table 5.2. The limit of the mould design for this mould shape without wrinkles corresponds to the mould C. The simulation setup of the mould C is illustrated in Figure 5.2. Thickness and shear angle distributions are shown in Figure 5.3. The highest predicted shear angle was 24 degrees and the highest thickness was 0.338 mm, with an increase of 9% in comparison to the initial thickness of 0.31 mm.

Table 5.2 Simulation results

Mould	A	B	C	D	E	F
α	45°	56°	74°	82°	76°	90°
β	33°	35°	47°	52°	55°	57°
Highest shear angle	15 °	21 °	24 °	50 °	60 °	83 °
Wrinkle	no	no	no	yes	yes	yes

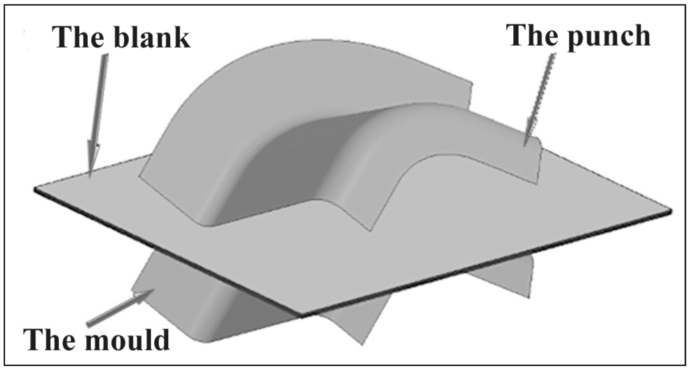

Figure 5.2 Simulation setup of mould C

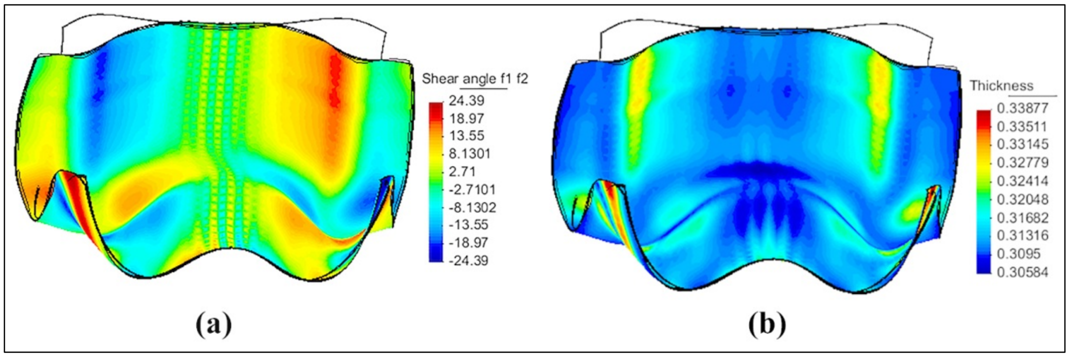

Figure 5.3 Forming predicted results of the mould C: (a) Shear angle; (b) Thickness

5.1.2 Mould design to avoid friction force

Based on the optimized angle α and angle β of the virtual mould C, a new virtual mould, named mould C2, was designed by taking into account the fabrication of the mould. This mould had the same forming angle β and angle α as the mould C. However, the surface of the mould C2, which was in fact the contact area between the mould and the laminate during the forming process, was different from the surface of the mould C, with two additional contact areas, the surface 1 and the surface 2 as illustrated in Figure 5.4. A forming simulation of the mould C2 was performed to study the effect of the friction at the surface 1 and the surface 2 on the forming process. Figure 5.5 shows the forming simulation setup. The predicted thickness and shear angle distributions are presented in Figure 5.6. The highest shear angle was up to 53 degrees in the forming prediction of the mould C2, while it was only 24 degrees in the forming prediction of the mould C. The highest thickness was 0.5216 mm, an increase of more than 68 per cent in comparison to the initial thickness of 0.31 mm. It is necessary to minimize the areas of the surface 1 and the surface 2 to reduce to the friction force that was created by the contact between these surfaces and the laminate during the forming process.

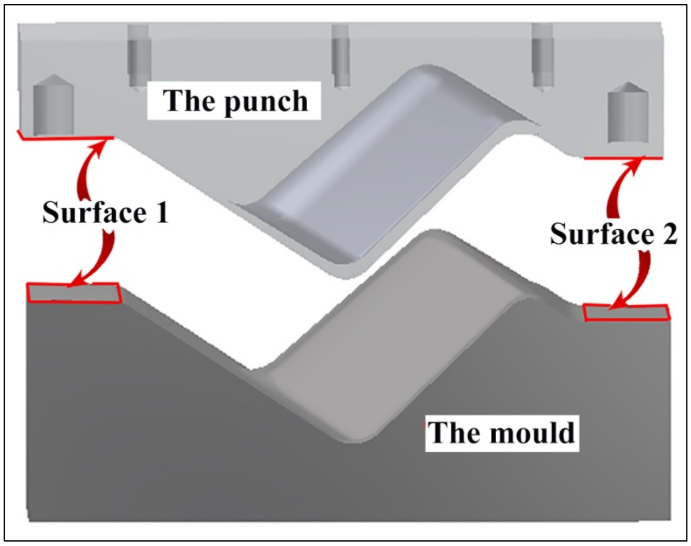
The punch
Surface 1
Surface 2
The mould

Figure 5.4 Mould C2

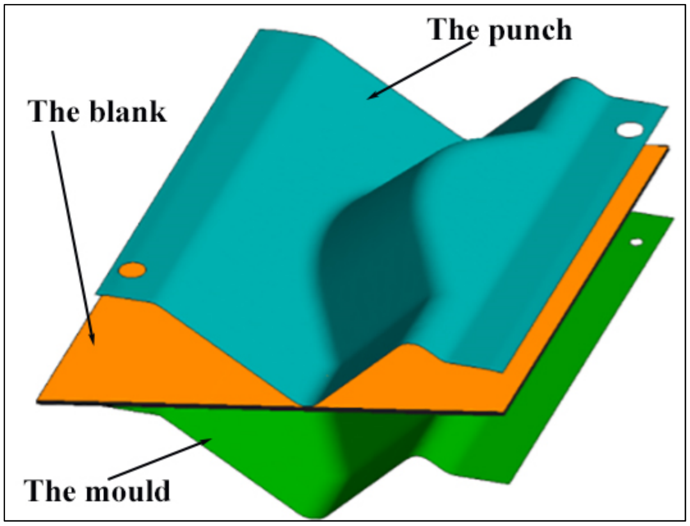
The punch
The blank
The mould

Figure 5.5 Simulation setup for mould C2

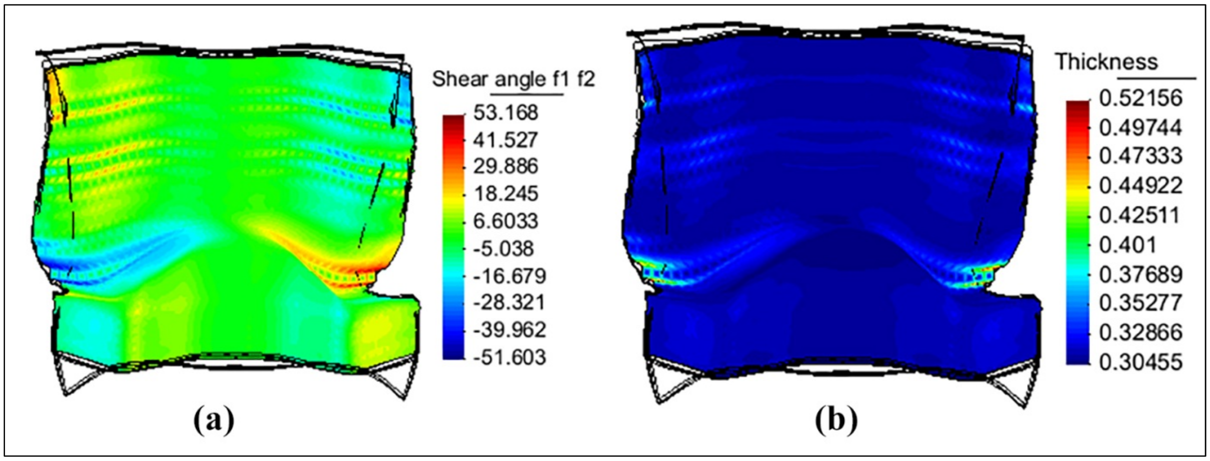

Figure 5.6 Forming prediction of the mould C2: (a) Shear angle; (b) Thickness

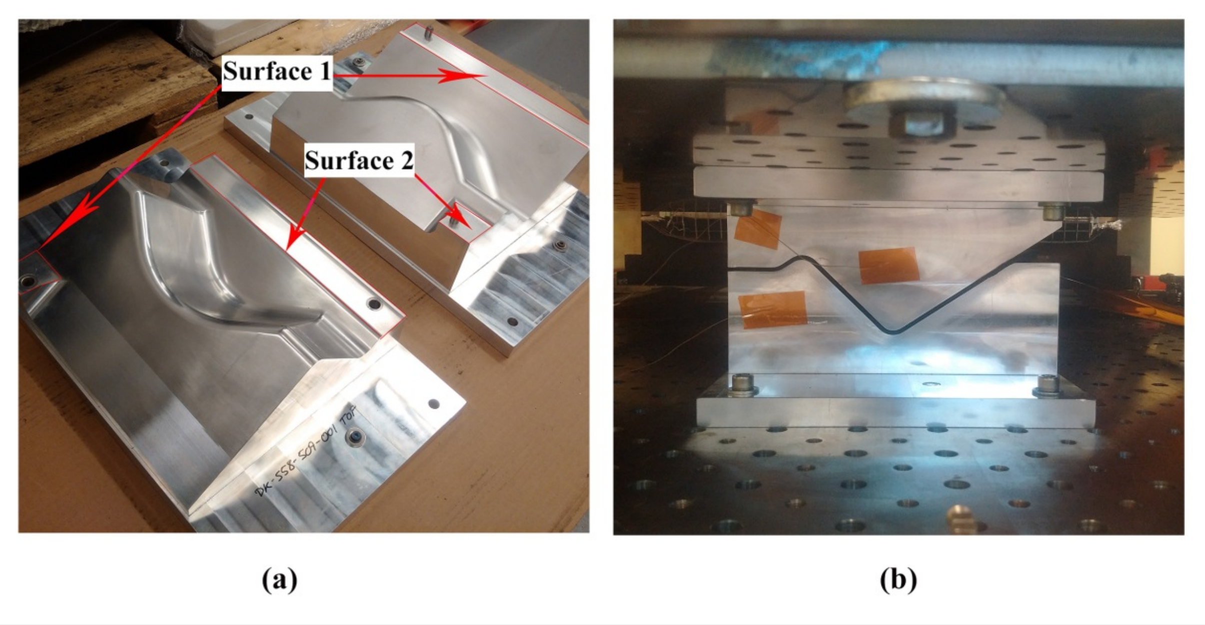

Figure 5.7 Real mould design (a) Two half- moulds; (b) The mould installed in the press

A real mould as shown in Figure 5.7 was fabricated with the minimized areas of the surface 1 and the surface 2 to reduce the friction force. However, due to the presence of the two guiding pins, a part of the surface 1 and surface 2 could not be removed, as depicted in Figure 5.8. Due to the limitation of this project, the size of the mould could not be changed and the impact of the pin locations on the forming results was inevitable.

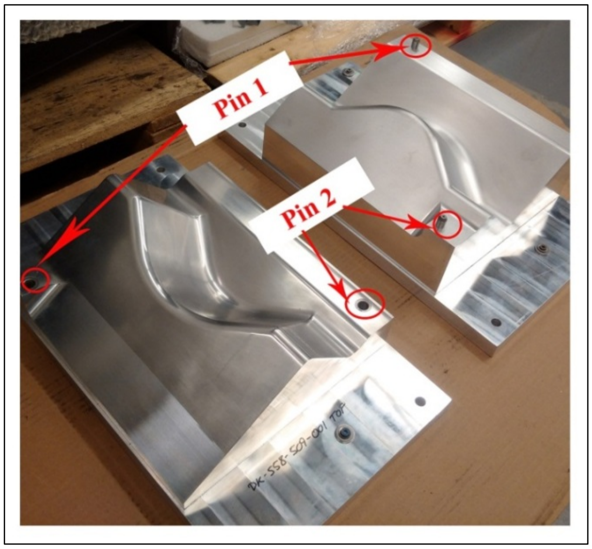

Figure 5.8 Pin locations

Figure 5.9(a) presents the forming simulation setup. The laminate was modelled as 280 mm long and 267 mm wide, exactly the same as the real blank used in the experiment. The effect of gravity on the laminate was also modelled as shown in Figure 5.9(b), where the sagging of the laminate was visible. Wrinkles and high shear angles appeared in both experimental and predicted results as presented in Figure 5.10(a) and Figure 5.10(b), respectively. It was remarked that wrinkles appeared along the direction between pin 1 and pin 2 as depicted in Figure 5.10(a).

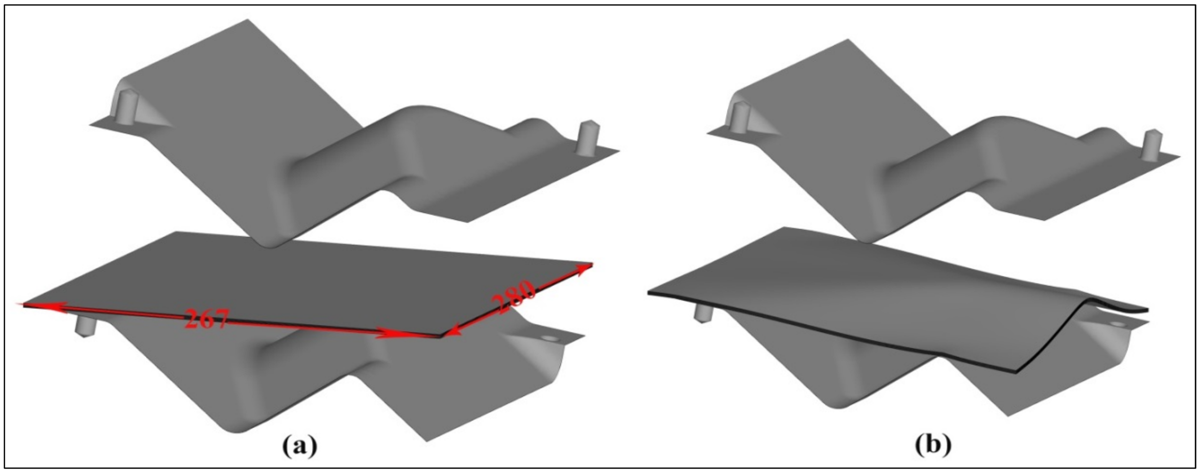

Figure 5.9 Simulation setup: (a) Simulation setup; (b) The effect of gravity

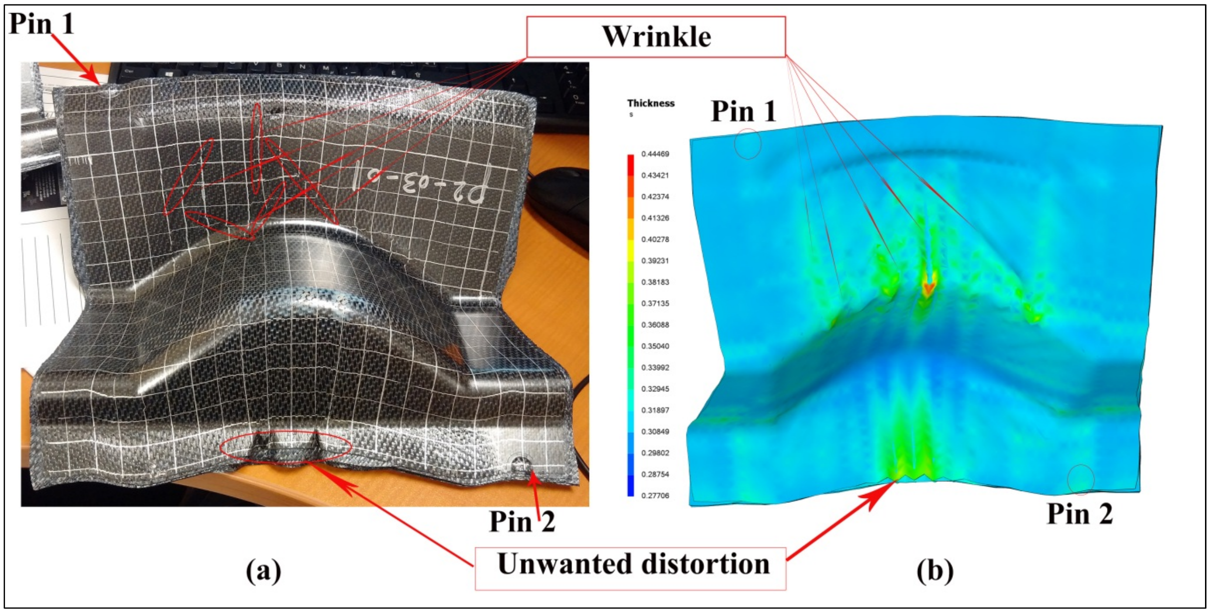
Pin 1
Wrinkle
Thickness
s
0.44469
0.43421
0.42374
0.41326
0.40278
0.39231
0.38183
0.37135
0.36088
0.35040
0.33992
0.32945
0.31897
0.30849
0.29802
0.28754
0.27706
Pin 1
P2-03-01
Pin 2
Pin 2
Unwanted distortion
(a)
(b)

Figure 5.10 Result comparison: (a) Experiment; (b) Simulation

The highest predicted thickness was up to 0.4121 mm as illustrated in Figure 5.11(a), an increase of thirty-three per cent over the initial thickness of 0.31 mm. The predicted fiber shear angle was up to 41 degrees as shown in Figure 5.11(b).

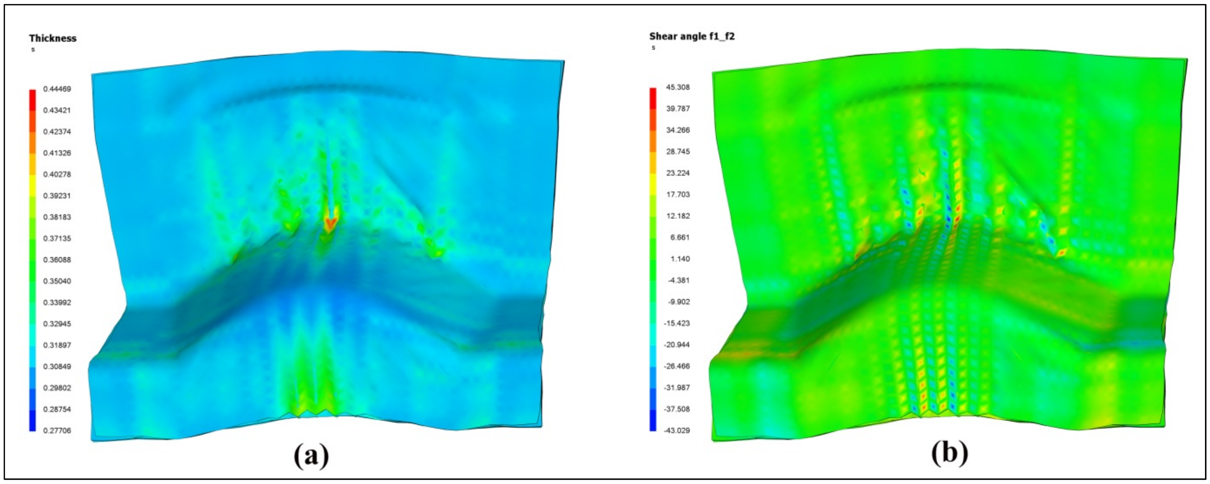
Thickness
s
0.44469
0.43421
0.42374
0.41326
0.40278
0.39231
0.38183
0.37135
0.36088
0.35040
0.33992
0.32945
0.31897
0.30849
0.29802
0.28754
0.27706
Shear angle f1_f2
s
45.308
39.787
34.266
28.745
23.224
17.703
12.182
6.661
1.140
-4.381
-9.902
-15.423
-20.944
-26.466
-31.987
-37.508
-43.029
(a)
(b)

Figure 5.11 Predicted result: (a) Thickness; (b) Shear angle

Figure 5.12 illustrates the contact between the laminate and the mould surfaces. The gap between two half-moulds at the pin locations was smaller than the gap at other locations on this surface. The friction force was higher at the pin locations. This could lead to the appearance of wrinkles. On the other hand, the formed part was unsymmetrical due to the effects of the pins. And this was prone also to wrinkles.

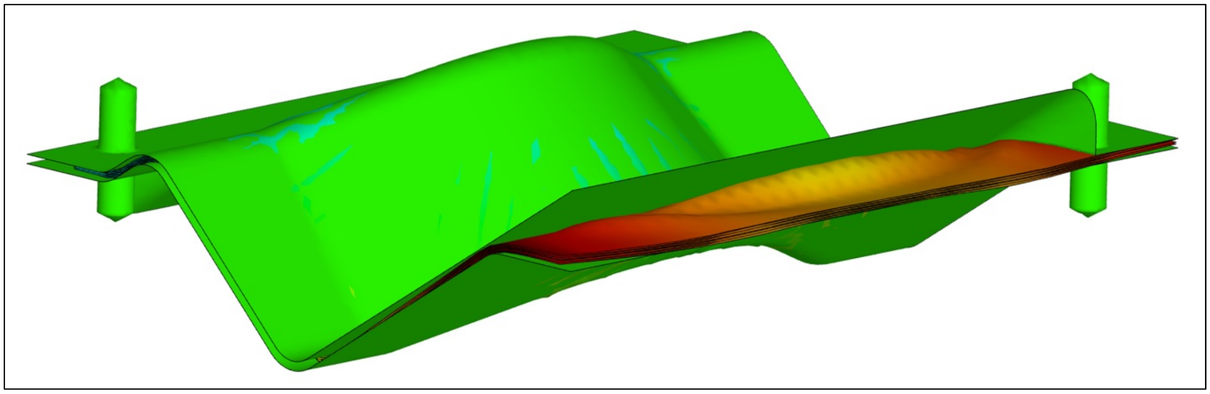

Figure 5.12 Contact between the blank and the mould

5.2 Mould design for stamp forming (phase III) with an eight-layer laminate

Based on the data in the previous paragraphs, a virtual mould for the forming of phase III was designed as demonstrated in Figure 5.13. The size of the mould was large enough to avoid contact between the laminate and the pin locations during the forming process, as illustrated in Figure 5.13(b), where the formed part was located entirely inside the mould. A forming simulation had been performed to predict the forming results before the mould was fabricated. Figure 5.14 shows the forming simulation setup. The eight-layer laminate blank was modelled as 190 mm long and 180 mm wide with the stacking sequence [(0,90)/(±45)/(±45)/(0,90)]s.

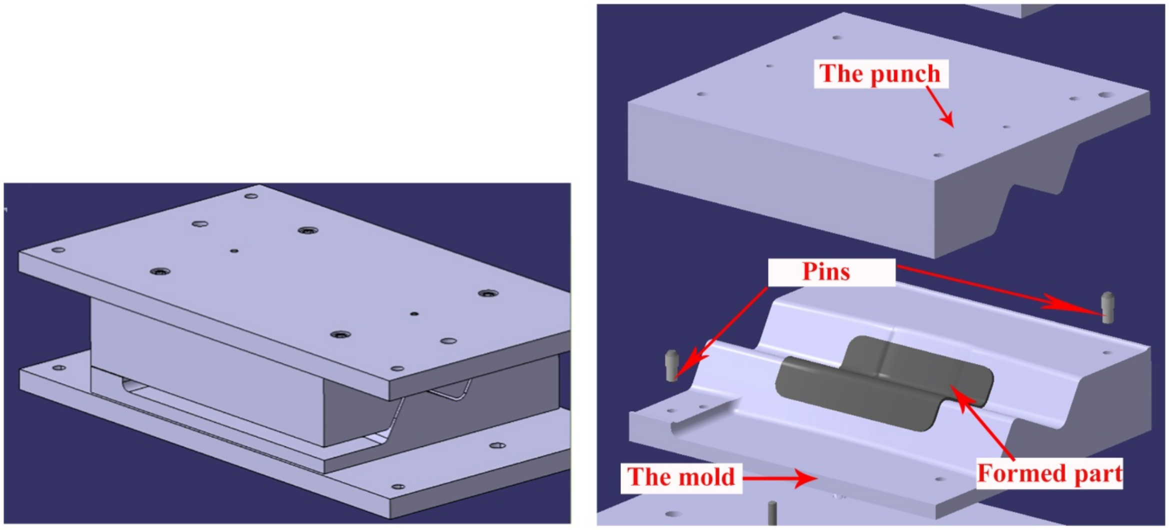

(a)

(b)

Figure 5.13 Phase III mould design: (a) Mould design; (b) Virtual formed part

In this design, the unnecessary constraints between the laminate and the mould surfaces have been removed as shown in Figure 5.15 (a), where the gap between the punch surface and the bottom mould surface at these areas was large enough to avoid contact between the laminate and the mould surfaces. The predicted shear angles are presented in Figure 5.15(b). The highest shear angle was just 8.6 degrees. It was observed that the formed surfaces were very smooth, free of wrinkles or unwanted distortions.

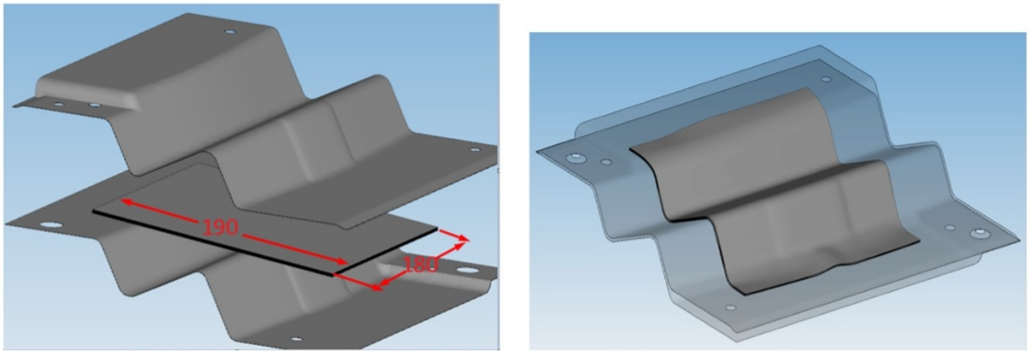

(a)

(b)

Figure 5.14 Forming simulation: (a) Simulation setup; (b) General deformation

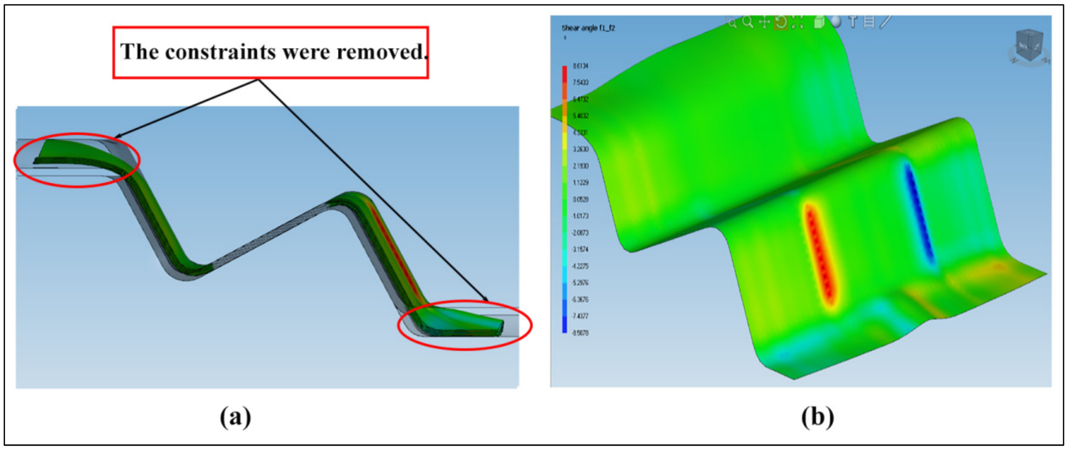
The constraints were removed.
Shear angle f1_f2
8.6134
7.5433
6.4732
5.4032
4.3331
3.2630
2.1930
1.1229
0.0528
-1.0173
-2.0873
-3.1574
-4.2275
-5.2976
-6.3676
-7.4377
-8.5078
(a)
(b)

Figure 5.15 Simulation results: (a) Closed mould; (b) Shear angle values

Since the predicted results for the new design were very good, the mould was fabricated and the forming experiment was performed as shown in Figure 5.16. The quality of the formed part agreed very well with the predicted results. The surfaces were very smooth without wrinkles. Sample was cut to measure the thickness using a digital calliper as shown in Figure 5.17. Very good agreements between the experimental and predicted results were found also in term of thickness and shear angles as presented in Figure 5.18 and Figure 5.19, respectively. It was observed that the highest shear angle was only 7 degrees. The highest thickness was 2.49 mm, an increase of less than 1% in comparison to the initial thickness of 2.48 mm.

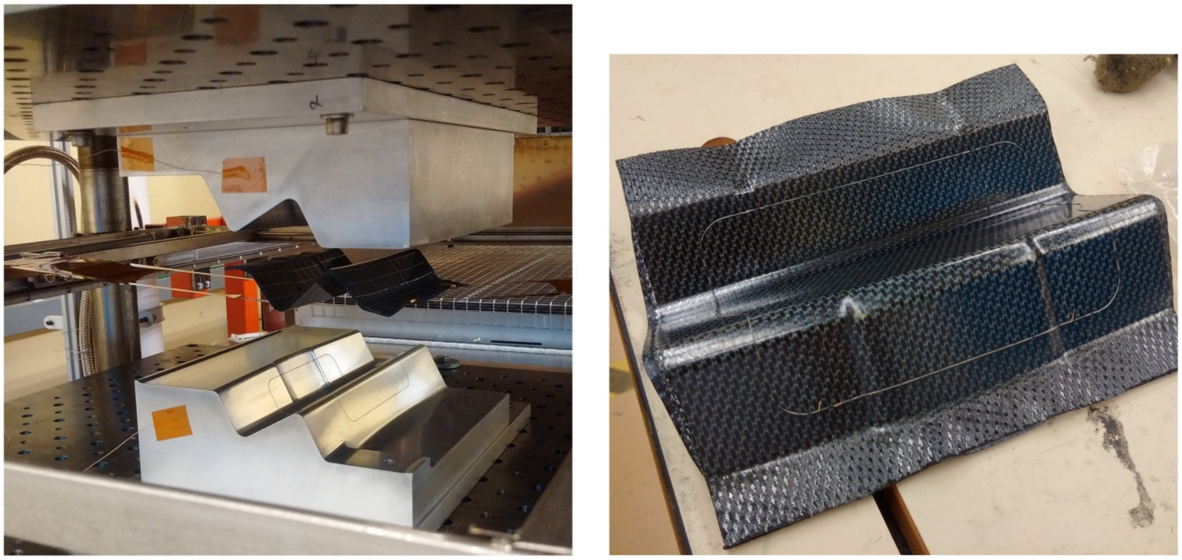

(a) (b)

Figure 5.16 Experiment: (a) Forming process, (b) Final shape

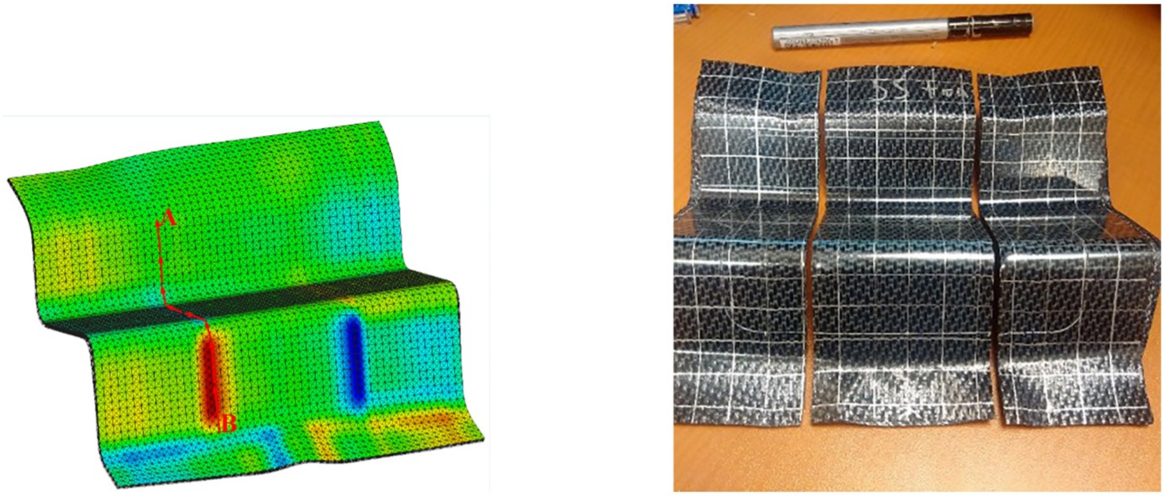

(a) (b)

Figure 5.17 Measurement: (a) Measurement positions; (b) Sample cutting lines

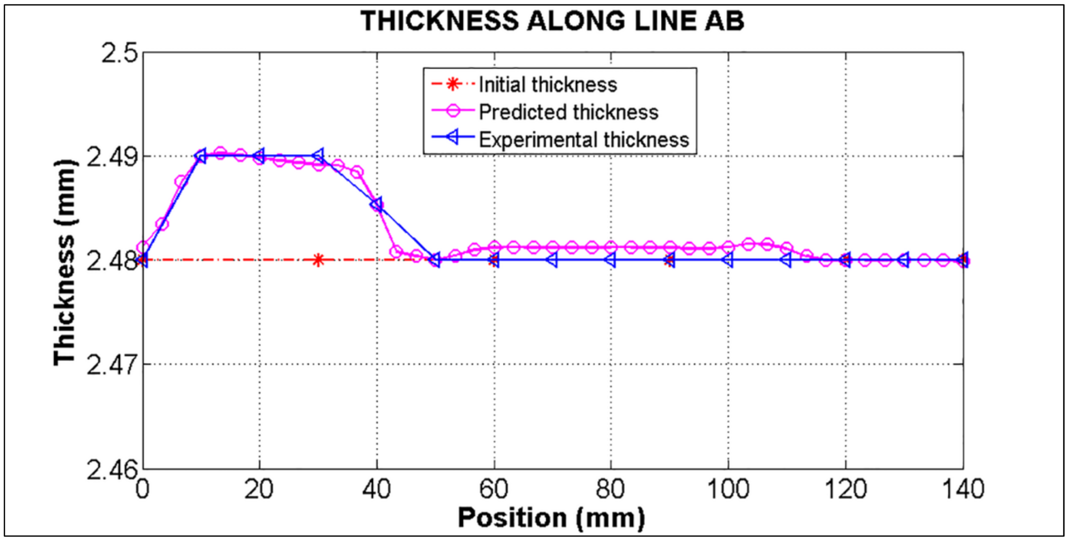

Figure 5.18 Thickness comparison

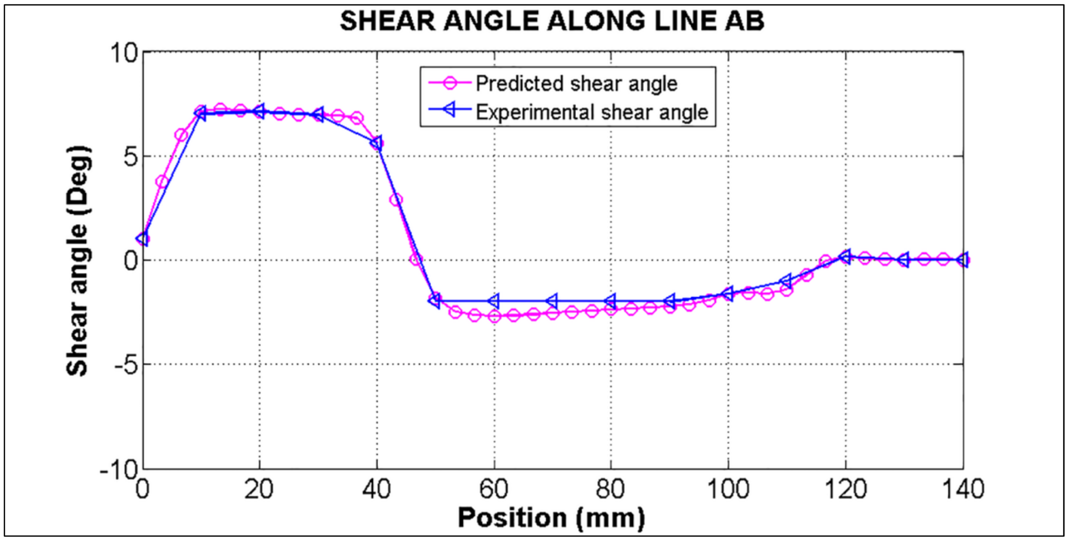

Figure 5.19 Shear angle comparison

CONCLUSIONS AND PERSPECTIVES

Stamp forming of multi-layer laminates of PPS/CF composites was successfully performed in both experiment and numerical simulations for several geometries, from the single curvature shape (phase I) to the double curvature shape (phase II) and the final complex shape (phase III). It was observed that:

- A good process window was determined for the forming of PPS/CF. Temperature and pressure are two indispensable parameters for the forming process.
- The formability of thermoplastic PPS/CF composite material was deeply investigated. More complex is the geometry, more difficult is the forming process, due the fact that the high shear angle value will create wrinkles and considerable thickness variation in the formed part. Through this study, a limit of the formability was detected.
- A good choice of primary models for different deformation mechanisms was an important factor for the success of forming simulations.
- It was challenging to get a full set of parameters for numerical models. These parameters were identified by material characterization tests. In this work, some of them were collected from the literature; some were obtained from characterization tests.
- It was very hard to get accurate values for some material parameters due to the complexity of the forming process. The inverse characterization using simulation-based multi-objective optimization technique was a very good way to determine these parameters.
- The optimal mould design for the forming of PPS/CF was successfully performed using numerical simulations to avoid defects. The numerical predictions agreed very well with the experimental results in term of thickness, fiber shear angles and wrinkle distribution.

It is remarked that forming simulations were successfully used as a rapid and low cost tool for mould design for the stamp-forming of PPS/CF composites. Having achieved this much, we need to consider a few research limitations for further developments:

- While material properties used in forming simulations were only measured at the highest temperature (330 °C) for PPS/CF material, the real temperature of the laminate dropped while transferring the laminate from the oven to the press and during the forming process.
- The thickness increase in the formed part was observed in this work. But it is still a scientific challenge for future study.
- The spring-back of the formed part when cooled down was not investigated in the current research yet. It is also an important subject of future research.

LIST OF References

Annin, B. D., Bel'metsev, N. F. and Chirkunov, Y. A. (2015). A group analysis of the equations of the dynamic transversely isotropic elastic model. *Journal of Applied Mathematics and Mechanics*.

Cross, M. M. (1965). Rheology of non-Newtonian fluids: a new flow equation for pseudoplastic systems. *J. Colloid Sci, 20* (5), 417-437.

Díez-Pascual, A. M. and Naffakh, M. (2012). Tuning the properties of carbon fiber-reinforced poly(phenylene sulphide) laminates via incorporation of inorganic nanoparticles. *Polymer, 53* (12), 2369-2378.

Eriksson, A. and Nordmark, A. (2014). Non-unique response of Mooney–Rivlin model in bi-axial membrane stress. *Computers & Structures, 144*, 12-22.

Gibson, R. F. (1994). *Principles of composite material mechanics*. United States of America: McGraw-Hill.

Haanappel, S. (2013). *Forming of UD fibre reinforced thermoplastics.* PhD.

Hamila, N. and Boisse, P. (2013). Locking in simulation of composite reinforcement deformations. Analysis and treatment. *Composites Part A: Applied Science and Manufacturing, 53*, 109-117.

He, L. W., Yan, S. P., Li, B. Q., Zhao, G. and Chu, J. R. (2013). Adhesion model of side contact for an extensible elastic fiber. *International Journal of Solids and Structures, 50* (16-17), 2659-2666.

Hussein, A., Hao, L., Yan, C. and Everson, R. (2013). Finite element simulation of the temperature and stress fields in single layers built without-support in selective laser melting. *Materials & Design, 52*, 638-647.

Jones, R. M. (1999). *Mechanics of composite materials* (2nd ed.): Taylor & Francis.

Liu, D., Zhu, Y., Ding, J., Lin, X. and Fan, X. (2015). Experimental investigation of carbon fiber reinforced poly(phenylene sulfide) composites prepared using a double-belt press. *Composites Part B: Engineering, 77*, 363-370.

Long, A. C. (2007). *Composites forming technologies*. Cambridge, England: Woodhead Publishing Ltd.

Nguyen, H. D., Deshaies, M. and Pham, X. T. (2015). *Simulation-assisted mold design for forming of thermoplastic PPS/CF composites*. Communication présentée au CASI-GARDN AERO Conference (AERO 2015) Montreal, Canada.

Robert, H. T., Dell, K. A. and Leo, A. (1994). *Manufacturing Processes Reference Guide*: Industrial Press Inc.

Spencer, A. J. M. (2000). Theory of fabric-reinforced viscous fluids. *Composites: Part A, 31*, 1311-1321.

Ten Thije, R. (2007). *Finite element simulations of laminated composite forming process* PhD, University of Twente

Ten Thije, R. (2014). ANIFORM Version 3.0. Page consultée de www.aniform.com.

Ten Thije, R. and Haanappel, S. (28-30 March 2011). *Muliti-layer thermoplastic composites manufacturing processes: simulations and experiments*. Communication présentée au SAMPE Europe International Conference & Forum, Paris, France.

Ten Thije, R. H. W., Akkerman, R. and Huétink, J. (2007). Large deformation simulation of anisotropic material using an updated Lagrangian finite element method. *Computer Methods in Applied Mechanics and Engineering, 196* (33-34), 3141-3150.

Trudel-Boucher, D. (2005). *Thermoformage d'un composite a fibres continues polypropylene/fibres de verre.* Ecole Polytechnique.